Accepted Manuscript

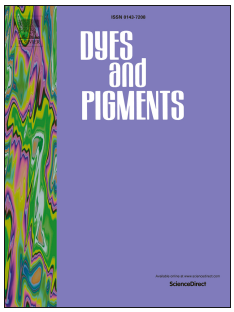

Solution-processable small molecules for bulk heterojunction ambipolar thin-film transistors and complementary-like inverters

Dongil Ho, Sureshraju Vegiraju, Donghee Choi, Chang-Hui Cho, Guhyun Kwon, Po-Chun Huang, Gene-Hsiang Lee, Taeshik Earmme, Shueh Lin Yau, Ming-Chou Chen, Choongik Kim

PII: S0143-7208(18)32176-4

DOI: https://doi.org/10.1016/j.dyepig.2018.12.054

Reference: DYPI 7259

To appear in: *Dyes and Pigments*

Received Date: 1 October 2018

Revised Date: 23 December 2018

Accepted Date: 24 December 2018

Please cite this article as: Ho D, Vegiraju S, Choi D, Cho C-H, Kwon G, Huang P-C, Lee G-H, Earmme T, Yau SL, Chen M-C, Kim C, Solution-processable small molecules for bulk heterojunction ambipolar thin-film transistors and complementary-like inverters, *Dyes and Pigments* (2019), doi: https://doi.org/10.1016/j.dyepig.2018.12.054.

Solution-processable small molecules for bulk heterojunction ambipolar thin-film transistors and complementary-like inverters

Dongil Ho,[a,1] Sureshraju Vegiraju,[b,1] Donghee Choi,[a] Chang-Hui Cho,[b] Guhyun Kwon,[a] Po-Chun Huang,[b] Gene-Hsiang Lee,[c] Taeshik Earmme,[d] Shueh Lin Yau,[b] Ming-Chou Chen,*[,b] and Choongik Kim*[,a]

[a] D. Ho, D. Choi, G. Kwon, Prof. C. Kim,

Department of Chemical and Biomolecular Engineering, Sogang University, Mapo-gu, Seoul, 04107 Republic of Korea

E-mail: choongik@sogang.ac.kr

[b] Dr. S. Vegiraju,+ Prof. M.-C. Chen, C.-H. Cho, P.-C. Huang, Prof. S. L. Yau

Department of Chemistry and Research Center of New Generation Light Driven Photovoltaic Modules,, National Central University, Taoyuan, 32001 Taiwan

E-mail: mcchen@cc.ncu.edu.tw

[c] Dr. G.-H. Lee

Instrumentation Center National Taiwan University Taipei 10617, Taiwan

[d] Prof. T. Earmme

Department of Chemical Engineering, Hongik University, Mapo-gu, Seoul, 04066 Republic of Korea.

[1] These authors contributed equally to this work.

Keywords: organic thin-film transistors; organic semiconductor; bithiophene; bulk heterojunction transistors; CMOS inverter

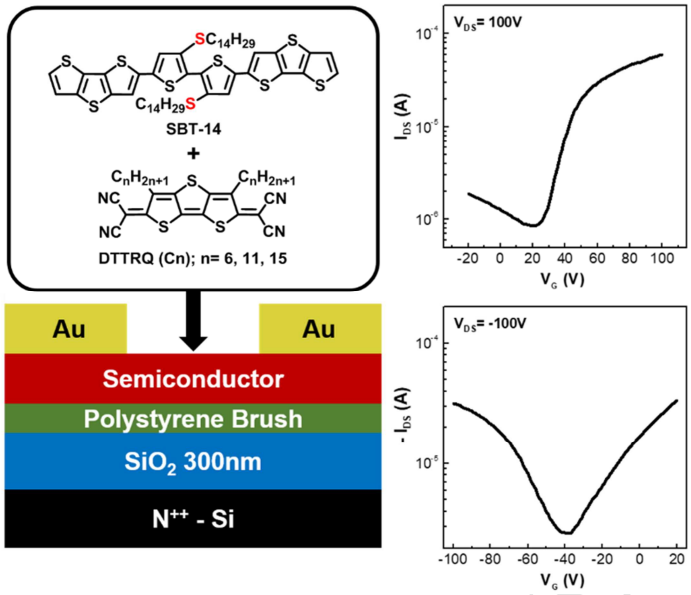

Table of Contents

Abstract

Solution-processable thioalkylated bithiophene derivatives with different lengths of side chains (**SBT-n**; **n** = **10**, **12**, **14**, **16**, **18**) have been synthesized and characterized as p-channel organic semiconductors for thin-film transistors (TFTs). Based on a combination of the highest performing SBT derivative (**SBT-14**) and quinoidals (**DTTRQ**s) as p- and n-channel materials, solution-processed small-molecular bulk heterojunction (BHJ) ambipolar thin-film transistors were fabricated, and the resulting devices showed air-stable and high ambipolar performance with well-balanced electron and hole mobilities as high as 0.70 cm^2 V^{-1} s^{-1} and 0.21 cm^2 V^{-1} s^{-1}, respectively. Furthermore, complementary-like inverters comprising two ambipolar thin-film transistors were demonstrated, which exhibited a high voltage gain of up to 81. Our study clearly demonstrated that side chain engineering of small molecular organic semiconductors had a significant influence on the electrical performance of TFTs and BHJ transistors, as well as complementary-like inverters.

1. Introduction

Organic electronics have been developed over the last few decades, with the advantages of large area processability at low cost for various applications, such as organic thin-film transistors (OTFTs), organic light-emitting diodes (OLEDs), organic photovoltaics (OPVs), and chemical sensors [1-11]. These developments were made possible through the design and synthesis of many new π-conjugated polymeric and small molecular organic semiconductors [12-24]. Among these, solution-processable small molecules with high performance and ambient stability have attracted interest due to their unique advantages of versatile molecular structure, simple synthesis, easy purification, high purity, and synthetic

reproducibility [25-30]. Aromatic building blocks with good π-conjugation are used for the molecular design of these semiconductors as they offer optimal charge transport, and alkyl chain substitutions are used for solution processability [31-36]. Regarding the conjugated heterocyclic aromatics, fused thiophenes have drawn interest due to their planar backbone structure with strong π–π stacking and intermolecular S-S interactions, which enhances the neighboring molecular orbital overlapping, and the resulting charge transport behavior [37-50].

The study of compounds with ambipolar charge transport is an important part of the development of organic semiconductors. Since both hole and electron transport is feasible for ambipolar TFTs, they can be applied in complementary metal-oxide semiconductor (CMOS)-like inverters for logic circuits [51-58]. Although inverters can be constructed using two complementary transistors in a CMOS configuration, CMOS-like inverters using ambipolar materials need only a single ambipolar semiconductor layer. Therefore, there is no need to pattern separate semiconductors, making it a cost-effective fabrication process for the implementation of electrical circuits.

Compared with the high hole and electron mobilities achieved for unipolar small molecular and polymeric organic semiconductors, small molecular ambipolar organic materials showed rather insufficient performance [59-61]. This is due to the difficulty in tuning the balanced energy levels with the work function of the metal electrodes, as well as the device instability in ambient conditions [62-64]. Charge carriers from the electrodes must be capable of transporting to both the HOMO and LUMO levels of ambipolar materials. For instance, through the combination of electron donor and acceptor building blocks in a molecular unit, semiconducting polymers could accomplish proper energy levels with good ambipolar characteristics [65-72]. Although there have been a few recent reports on

ambipolar polymeric semiconductors with carrier mobility > 1.0 $cm^2 V^{-1} s^{-1}$ for both hole and electron [73-76], there are few reports on ambipolar small molecular semiconductors, and they showed relatively low mobilities. For instance, ambipolar silylethynylated N-heteropentacenes were reported with a hole mobility up to 0.22 $cm^2 V^{-1} s^{-1}$ (in ambient air) and electron mobility up to 1.1 $cm^2 V^{-1} s^{-1}$ (under a vacuum), respectively [59]. Fluorine-functionalized asymmetric tetraceno[2,3-*b*]thiophenes were reported to exhibit maximum hole and electron mobilities of 0.071 and 0.37 $cm^2 V^{-1} s^{-1}$ under a nitrogen environment, respectively [60]. Balanced ambipolar mobilities of pentacene derivatives were reported with hole and electron mobilities of up to 0.51 and 0.46 $cm^2 V^{-1} s^{-1}$ under nitrogen atmosphere, respectively [61].Although there have been a few reports on ambipolar small molecular semiconductors, the semiconducting films were mostly fabricated via vacuum deposition and experienced decreased performance in ambient conditions [59-61].

Another promising method to form ambipolar semiconductor films is to blend two organic semiconductors with different polarities, resulting in a bulk heterojunction (BHJ) structure [77-81]. The ambipolar organic bulk heterojunction thin-film transistors can simply be fabricated via a single solution process, which could reduce the fabrication cost of electrical circuits. Reports on small molecular blend ambipolar organic semiconductors are also rare, and those that have been published show relatively low mobilities. For instance, ambipolar characteristics with hole and electron mobilities of 0.01 and 0.001 $cm^2 V^{-1} s^{-1}$, respectively, were reported by blending naphthalene diimide (NDI) derivatives [82]. An optimized blend of thieno[3,2-b;4,5-b']dithiophene (BTDT) derivative with *n*-channel semiconductor, C_{60}, was reported to result in a BHJ ambipolar transistor with balanced carrier mobilities for holes and electrons of 0.03 and 0.02 $cm^2 V^{-1} s^{-1}$, respectively [40]. A recent study by Zhu et al. reported ambipolar behavior for a donor (DPTTA) and acceptor

(DTTCNQ) charge transfer complex with hole and electron mobilities of 0.77 and 0.24 $cm^2 V^{-1} s^{-1}$, respectively, for single crystal field-effect transistors [83]. However, to the best of our knowledge, there are no example of solution-processed small molecular blends demonstrating balanced ambipolar characteristics with both hole and electron mobilities higher than 0.1 $cm^2 V^{-1} s^{-1}$ in ambient.

To this end, a bithiophene-based solution processable p-type semiconducting SBT series was synthesized in this study (**Fig. 1**). Different length of alkyl chains connected to the bithiophene moiety was employed to deduce the relationship between the length of the side chain and the resulting charge transport characteristics. Furthermore, organic thin-film transistors (OTFTs) of each series were fabricated, and their electrical performance was investigated. In particular, **SBT-14** with tetradecyl thioalkyl chain substituents ($-SC_{14}H_{29}$) exhibited promising p-type characteristics with hole mobility up to 0.30 $cm^2 V^{-1} s^{-1}$, and was blended with n-type semiconductor material **DTTRQ**s with various alkyl substituents (**DTTRQ (C3), (C6)**, **(C11)**, and **(C15)**) to construct bulk heterojunction (BHJ) thin-film transistors (**Fig. 2**), which exhibited ambipolar characteristics. Fused thienoquinoids were selected as n-channel materials for blends, since they have been reported to exhibit high electrical performance with electron mobility as high as 0.90 $cm^2 V^{-1} s^{-1}$ in ambient [84]. Furthermore, **DTTRQ**s employed in this study exhibit high solubility enough for solution process due to the presence of alkyl chains, while solubilities of many quinoidal molecules are too poor to fabricate devices via solution process due to the strong π–π stacking among molecules [84]. Through the use of chain-modulated **DTTRQ**s and optimization of the blend ratio between **SBT-14** and **DTTRQ**s, the BHJ transistors showed ambipolar device operations with balanced electron and hole mobilities as high as 0.70 and 0.21 $cm^2 V^{-1} s^{-1}$, respectively. To the best of our knowledge, this result is one of the highest balanced

ambipolar characteristics for solution-processed small molecules reported to date. Finally, ambipolar BHJ transistors based on **SBT-14** and **DTTRQ (C11)** were employed for the fabrication of complementary-like inverters, and the resulting devices showed a high voltage gain of up to 81.

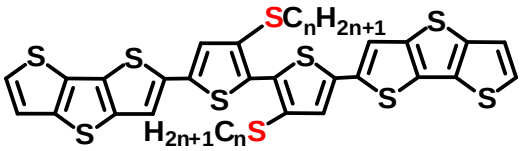

SBT- n
n = 10; 1
12; 2
14; 3
16; 4
18; 5

Fig. 1. Chemical structure of the synthesized SBT series employed in this study.

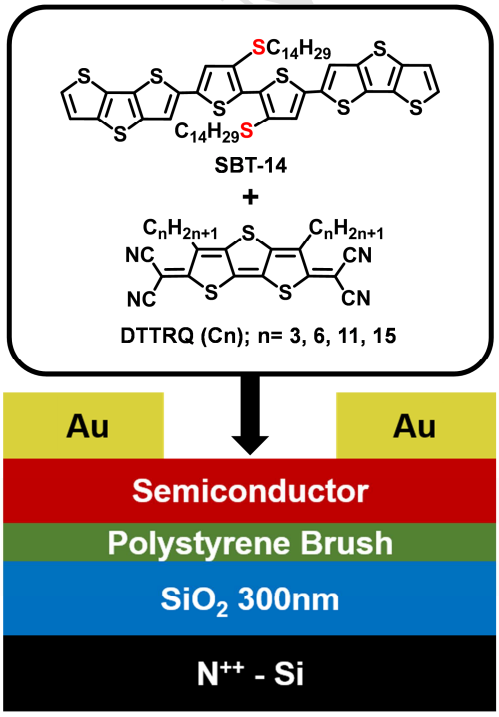

Fig. 2. The device structure of bulk heterojunction ambipolar transistors employed in this study with molecular structures of **SBT-14** and four **DTTRQ**s.

2. Experimental

2.1. General Methods

^{1}H and ^{13}C NMR were recorded using a Bruker 500 or 300 instrument for all materials, with reference to solvent signals. Mass spectrometric data were obtained with a JMS-700 HRMS instrument. Differential scanning calorimetry (DSC) was carried out under nitrogen on a Mettler DSC 822 instrument (scanning rate of 10 °C min^{-1}). Thermogravimetric analysis (TGA) was carried out using a Perkin Elmer TGA-7 thermal analysis system, using dry nitrogen as a carrier gas at a flow rate of 10 mL min^{-1} (heating rate of 10 °C min^{-1}), and the reported decomposition temperatures represent the temperature observed at 5 % mass loss. UV-Vis absorption was carried out in the indicated solvents at room temperature with a JASCO V-530 spectrometer. Differential pulse voltammetry (DPV) experiments were performed with a conventional three-electrode configuration (a platinum disk working electrode, an auxiliary platinum wire electrode, and a non-aqueous Ag reference electrode, with a supporting electrolyte of 0.1 M tetrabutylammoniumhexafluorophosphate ($TBAPF_6$) in the specified dry solvent) using a CHI621C Electrochemical Analyzer (CH Instruments). All electrochemical potentials were referenced to an Fc^{+}/Fc internal standard (at 0.6 V). Crystallographic data (excluding structure factors) for the structure(s) reported in this paper were deposited with the Cambridge Crystallographic Data Centre as supplementary publication with the numbers CCDC 1819944 for SBT-10 and CCDC 1819945 for DTTRQ-3.

2.2. Synthesis

Starting materials (from Aldrich, Arco, or TCI Chemical Co.) were of reagent grade and used without further purification unless otherwise indicated. Reaction solvents (toluene, ether, and tetrahydrofuran) were distilled under nitrogen from sodium/benzophenoneketyl,

and halogenated solvents were distilled from CaH_2. 3-bromothiophene (**7**), 3,3'-dibromo-2,2'-bithiophene (**8**), 3,3'-bis(alkylthio)-2,2'-bithiophene (**9**), 5,5'-dibromo-3,3'-bis(alkylthio)-2,2'-bithiophene (**10**), tributyl(dithieno[3,2-b:2',3'-d]thiophen-2-yl)stannane (**11**), and **SBT-14** were synthesized as reported previously [91]. DTTRQ derivatives were synthesized according to the previous report [84].

2.3. General Procedure for Stille Cross-Coupling Reactions to Final Targets (SBT-10 – 18)

Under anhydrous conditions, $Pd(PPh_3)_4$ (0.05 equiv) was added to a solution of dibrominated compounds (**10a-10e**; 1 equiv) and mono-stannylated dithienothiophene(**11**; 2.2 equiv) in dry toluene. The resulting mixture was refluxed overnight under nitrogen. After removal of solvent, the obtained residue was purified by column chromatography on silica gel with dichloromethane and hexanes as the eluents. It was then further purified by recrystallization in dichloromethane.

2.3.1. Synthesis of SBT-10

The title compound was obtained as a red solid (yield = 67%). Mp: 151 °C. ^{1}H NMR (300 MHz, $CDCl_3$): δ 7.41 (s, 2 H), 7.39 (d, *J* = 5.1 Hz, 2 H), 7.29 (d, *J* = 5.4 Hz, 2 H), 7.19 (s, 2 H), 2.88 (t, *J* = 7.2 Hz, 4 H), 1.68-1.58 (m, 4 H), 1.41-1.37 (m, 4 H), 1.32-1.21 (m, 24 H), 0.86-0.81 (m, 6 H). ^{13}C NMR (125 MHz, $CDCl_3$): δ 141.94, 141.63, 137.12, 136.77, 132.57, 131.75, 130.91, 129.94, 127.16, 126.41, 120.80, 117.45, 36.44, 31.91, 29.60, 29.54, 29.36, 29.23, 28.78, 22.68, 14.10. HRMS (*m/z*, FAB+) calcd for $C_{44}H_{50}S_{10}$ 898.1120, and 898.1114 was found.

2.3.2. Synthesis of SBT-12

he title compound was obtained as a red solid (yield = 48%). Mp: 136 °C. ^{1}H NMR (500 MHz, $CDCl_3$): δ 7.41 (s, 2 H), 7.38 (d, *J* = 5 Hz, 2 H), 7.29 (d, *J* = 5.5 Hz, 2 H), 7.19 (s,

2 H), 2.88 (t, *J* = 7.5 Hz, 4 H), 1.64-1.59 (m, 4 H), 1.39-1.35 (m, 4 H), 1.32-1.21 (m, 32 H), 0.87-0.84 (m, 6 H). ^{13}C NMR (125 MHz, $CDCl_3$): δ 141.95, 141.63, 137.14, 136.78, 132.60, 131.77, 130.92, 129.95, 127.19, 126.41, 120.80, 117.46, 36.44, 31.91, 29.70, 29.65, 29.60, 29.53, 29.36, 29.22, 28.76, 22.68, 14.04. HRMS (*m/z*, FAB+) calcd for $C_{48}H_{58}S_{10}$ 954.1746, and 954.1749 was found.

2.3.3. Synthesis of SBT-14

The title compound was obtained as a red solid (yield = 74%). Mp: 141 °C. ^{1}H NMR (300 MHz, $CDCl_3$): δ 7.42 (s, 2 H), 7.39 (d, *J* = 5.4 Hz, 2 H), 7.29 (d, *J* = 5.4 Hz, 2 H), 7.19 (s, 2 H), 2.29 (t, *J* = 7.5 Hz, 4 H), 1.68-1.58 (m, 4 H), 1.45-1.35 (m, 4 H), 1.32-1.21 (m, 40 H), 0.86 (t, *J* = 7.2 Hz, 6 H). ^{13}C NMR (125 MHz, $CDCl_3$): δ 142.04, 141.72, 137.19, 136.90, 132.79, 131.92, 131.01, 130.52, 127.32, 126.37, 120.79, 117.49, 36.51, 31.93, 29.70, 29.65, 29.61, 29.60, 29.34, 29.22, 28.79, 22.67, 14.05. HRMS (*m/z*, FAB+) calcd for $C_{52}H_{66}S_{10}$ 1011.2372, found 1011.2476.

2.3.4. Synthesis of SBT-16

The title compound was obtained as a red solid (yield = 43%). Mp: 129 °C. ^{1}H NMR (500 MHz, $CDCl_3$): δ 7.42 (s, 2 H), 7.39 (d, *J* = 5.0 Hz, 2 H), 7.29 (d, *J* = 5.0 Hz, 2 H), 7.19 (s, 2 H), 2.88 (t, *J* = 7.5 Hz, 4 H), 1.65-1.61 (m, 4 H), 1.40-1.38 (m, 4 H), 1.32-1.21 (m, 48 H), 0.88-0.85 (m, 6 H). ^{13}C NMR (125 MHz, $CDCl_3$): δ 141.95, 141.63, 137.13, 136.78, 132.60, 131.77, 130.92, 129.95, 127.19, 126.40, 120.79, 117.45, 36.44, 31.93, 29.70, 29.66, 29.60, 29.53, 29.36, 29.21, 28.76, 22.69, 14.11. HRMS (*m/z*, FAB+) calcd for $C_{56}H_{74}S_{10}$ 1066.2998, and 1066.2999 was found.

2.3.5. Synthesis of SBT-18

The title compound was obtained as a red solid (yield = 65%). Mp: 176 °C. ^{1}H NMR (300 MHz, $CDCl_3$): δ 7.42 (s, 2 H), 7.39 (d, *J* = 5.4 Hz, 2 H), 7.29 (d, *J* = 5.1 Hz, 2 H), 7.20

(s, 2 H), 2.88 (t, *J* = 7.5 Hz, 4 H), 1.68-1.58 (m, 4 H), 1.45-1.35 (m, 4 H), 1.32-1.21 (m, 56 H), 0.89-0.85 (m, 6 H). This material was not sufficiently soluble to collect ^{13}C NMR. HRMS (*m/z*, FAB+) calcd for $C_{60}H_{82}S_{10}$ 1122.3624, and 1122.3618 was found.

2. 4. Device fabrication

The OTFTs and complementary-like inverters were fabricated with the top contact/bottom gate (TC/BG) structure. The highly n-doped silicon wafers with thermally grown 300 nm oxide (areal capacitance; C_i =11.4 nF cm^{-2}) were cleaned via sonication in acetone for 10 min and treated by air plasma for 5 min (Harrick plasma, PDC-32G, 18 W). Organic semiconductor layers (single component or blend) were formed via solution-shearing on PS-brush-treated substrates. The PS-brush (M_w = 1.7 – 28 kg mol^{-1}) treatments were implemented following the general recipe [92]. The concentration of organic material solution, solvent type, substrate temperature, blending ratio, and shearing speed were optimized. The solution-sheared substrates were annealed in a vacuum at various temperature for 30 min to remove the residual solvent. The thicknesses of semiconductor layers for a single SBT layer (34 – 86 nm) and for blend organic films (31 – 60 nm) were measured using a profilometer (DEKTAK-XT, Brucker). The Au layers (50 nm) with various channel widths (W; 2000, 1000, and 500 μm) and lengths (L; 100 and 50 μm) were thermally evaporated to define the source and drain electrodes.

2.5. Device Characterization

The electrical performances of OTFTs and complementary-like inverters were characterized in ambient conditions at room temperature with a semiconductor parameter analyzer (Keithley 4200-SCS) equipped with a probe station. Carrier mobilities (μ) were

determined in the saturation regime by the standard relationship, $\mu_{sat} = (2I_{DS}L)/[WC_i(V_G-V_T)^2]$, ($I_{DS}$; source-drain current, L; the channel length, W; channel width, C_i; areal capacitance of the gate dielectric (11.4 nF cm^{-2}), V_G; gate voltage, V_T; threshold voltage). The microstructure and surface morphology of the semiconductor thin-films were measured by atomic force microscopy (AFM, NX10, Park systems) and wide-angle X-ray diffraction (XRD, Smartlab, Rigaku).

3. Results and discussion

3. 1. Synthesis

The **SBT** core was prepared in two steps, first the selective deprotonation of 3-bromothiophene (**7**) with LDA and then homocoupling in the presence of $ZnCl_2/CuCl_2$ to afford dibromobithiophene **8**. Next, lithium alkylthiolate anion was prepared by treating the corresponding alkanethiol with n-BuLi, and the nucleophilic substitution of **8** with lithium alkylthiolate in the presence of CuO/KI produces **9** after facile purification, with an overall yield >70%. The **SBT** core was dibrominated using n-bromosuccinimide, then end-capped with dithienothiophene (**DTT**), with a Stille cross coupling reaction of **10** with tributylstannyl-**DDT** (**11)** then used to produce the small molecules **SBT-10** – **18**, respectively (**Scheme 1**).

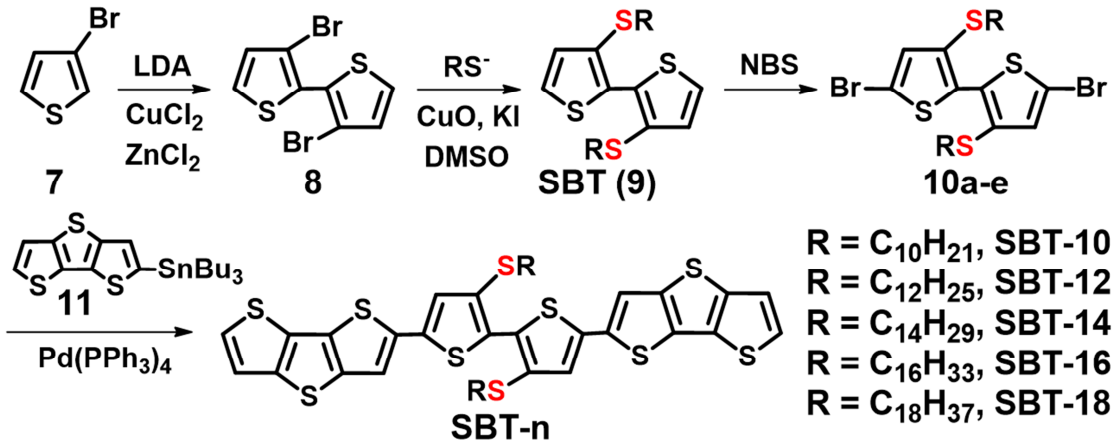

Scheme 1. Synthetic routes to the small molecules **SBT-10 – 18**

3. 2. Thermal, optical, and electrochemical properties

Thermal properties of SBT derivatives were investigated using thermogravimetric analysis (TGA) and differential scanning calorimetry (DSC). TGA revealed that the **SBT** compounds **1 – 5** exhibited good thermal stability, with ~5 wt % loss occurring at 319 to 352 °C (**Fig. S1**). Note that the two-connected alkyl chain breaking occurred during the thermal decomposition for all five **SBT** derivatives, which can be confirmed from their TGA weight loss percentages. DSC showed that **SBT** derivatives melted at above 129 °C (**Fig. S2)**. The data is summarized in **Table 1**. The UV-Vis absorption spectra of **SBT** derivatives in *o*-dichlorobenzene are shown in **Fig. 3a**. The absorption spectra of all compounds in solution state were almost identical and exhibited the maximum absorption wavelengths (λ_{max}) at 436-439 nm. The absorption maximum of **SBT-18** was slightly blue-shifted (~ 10 nm) compared to other **SBT**s. The absorption maxima of the UV-Vis absorption spectra for spin-coated films were slightly red-shifted (**Fig. S3**) compared to those in solution state, indicating the enhancement of molecular stacking in the solid state.

Table 1
Optical, Electrochemical, and Thermal Properties of SBT Derivatives. (T_m: melting temperature, T_d: decomposition temperature; 5%).

Compounds	T_m [°C]	T_d [°C]	λ_{max} [nm][a)]	Potential [V] [b)]		HOMO [eV] [c)]	LUMO [eV] [c)]
				E_{ox}	E_{red}		
SBT-10	151	333	437	0.87	-1.69	-5.07	-2.51
SBT-12	136	319	439	0.88	-1.71	-5.08	-2.49
SBT-14	140	352	436	0.87	-1.62	-5.07	-2.58
SBT-16	129	337	436	0.86	-1.69	-5.06	-2.51
SBT-18	134	339	426	0.88	-1.72	-5.08	-2.48

[a)] in *o*-$C_6H_4Cl_2$. [b)] by DPV in *o*-$C_6H_4Cl_2$ at 25 °C, E_{ox} = Oxidative potential, E_{red} = Reductive potential. [c)] HOMO = -(4.2+E_{ox}); LUMO = -(4.2+E_{red}).

The electrochemical properties were investigated by differential pulse voltammetry (DPVs) in *o*-dichlorobenzene at 25 ºC with a 0.1 M Bu_4NPF_6 solution, and Fc/Fc^+ was used as an internal standard calibrated at +0.60 eV. The oxidation and reduction potential curves are shown in **Fig. 3b** and **Fig. S4**, respectively, and the data is summarized in **Table 1**. The estimated DPV data show that the oxidation and reduction potentials are located at 0.86 – 0.88 V and -1.62 – -1.72 V, respectively. According to the equation: HOMO/LUMO = -(4.2 + E_{ox}/E_{red}), assuming ferrocene/ferrocenium oxidation at -4.8 eV, the highest occupied molecular orbital (HOMO) and lowest unoccupied molecular orbital (LUMO) energies of **SBT** derivatives were around -5.06 – -5.08 eV and -2.48 – -2.58 eV, respectively. The HOMO and LUMO energy levels of **SBT** derivatives were almost identical, irrespective of the thioalkyl side chain on the molecular backbone.

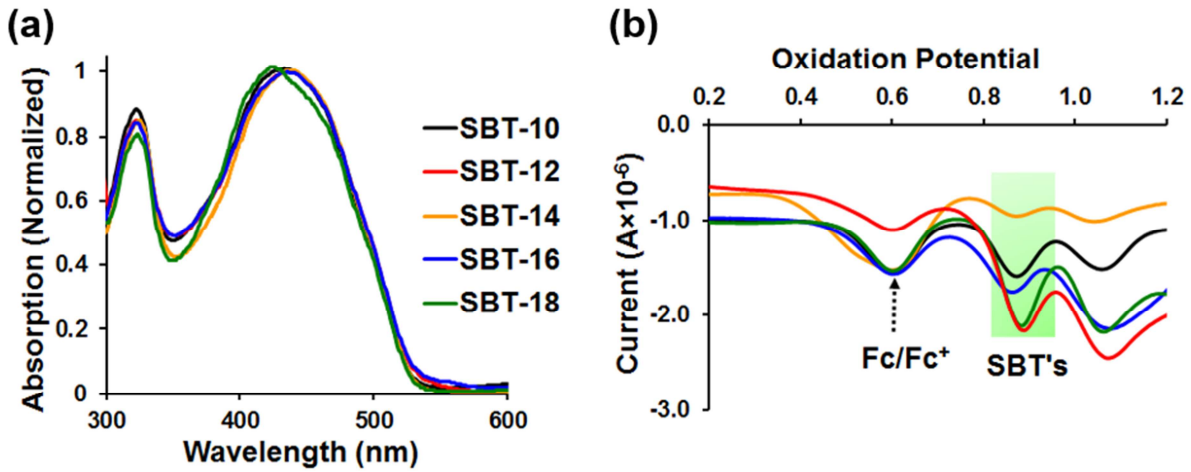

Fig. 3. (a) UV-Vis spectra and (b) DPV curves of **SBT** derivatives in o-dichlorobenzene solution.

3. 3. Single crystal analyses

Single crystals of **SBT-10** were obtained using a slow solvent evaporation method from solvent mixture (hexane and dichloromethane), and the crystal structures are shown in **Fig. 4** with the results of their analysis in **Table S1**. As seen in **Fig. 4a**, all four S atoms in the SBT unit are in one plane, and the intramolecular distance of S(Thio)··S(R) is ~3.07 Å. This value is below the sum of the van der Waals radii of two S atoms (~1.8 Å), suggesting that there are strong S(Thio)··S(R) intramolecular interactions. The alkyl chains are positioned opposite to each other and the two end-capped **DTT** fused-thiophene moieties have the dihedral angles of 7.2° (**Fig. 4b**) with the SBT unit. The molecular length of **SBT-10** was 23.8 Å, and the inter planar distance between the **SBT** molecules was ~ 3.48 Å (**Fig. 4c**). **Figs. 4d–f** show the molecular packing arrangements with slipping angles of 72° and 50°.

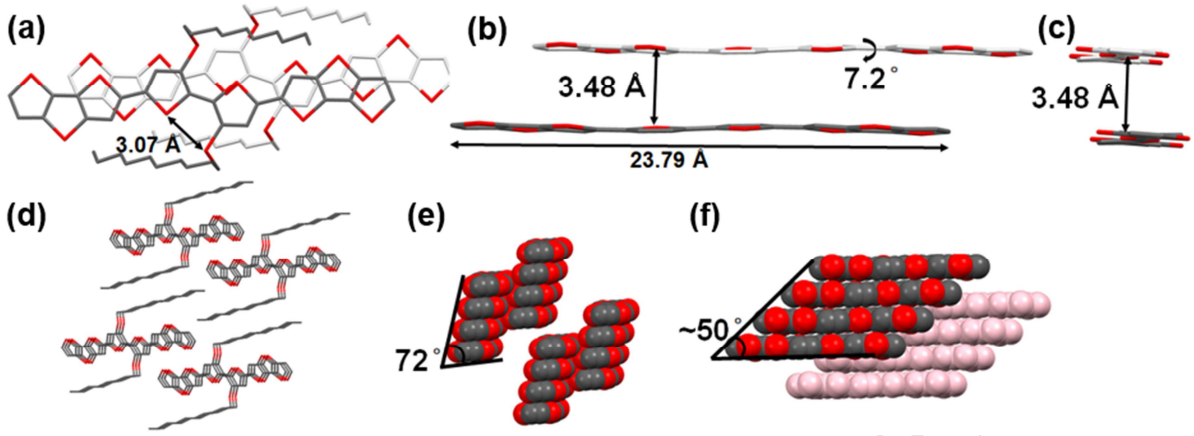

Fig. 4. Single crystal structures of the **SBT-10** (all hydrogen atoms have been omitted for clarity). Red and black colors indicate sulfur and carbon atoms, respectively. (a) Top view of two stacking **SBT-10** molecules. (b) Front view of two stacking **SBT-10** molecules. The interplanar distance between the **SBT-10** layers is ~ 3.48 Å (the alkyl chains are omitted). (c) Side view of two **SBT-10** molecules. (d) Packing orientation of alkyl chains (e–f) Molecular packing arrangement of **SBT-10** molecules with slipping angles of 72° and 50°.

Single crystalline propyl alkylated **DTTRQ-3** was also obtained from a solvent mixture of hexane and dichloromethane by slow evaporation of the solvent. Note that **DTTRQ-3** with shorter alkyl chains, compared to other **DTTRQ**s employed in this study, might give insight into the molecular arrangement of the corresponding compounds. As shown in **Fig. 5** and **Table S2**, the two CN groups were almost coplanar with the **DTT** main core, with small torsion angles of 4.5-5.7° and the molecular length was 13 Å (**Fig. 5b**). The molecule exhibited a slipped 1D stacking arrangement (**Fig. 5d**). The **DTTRQ** molecule was connected with the neighboring molecules through a “zig-zag” arrangement in the same layer, with short intermolecular S-N distances of 3.08 Å and 3.05 Å (**Fig. 5e**). The inter planar distance between the “zig-zag” layers was 3.40 Å (**Fig. 5f**).

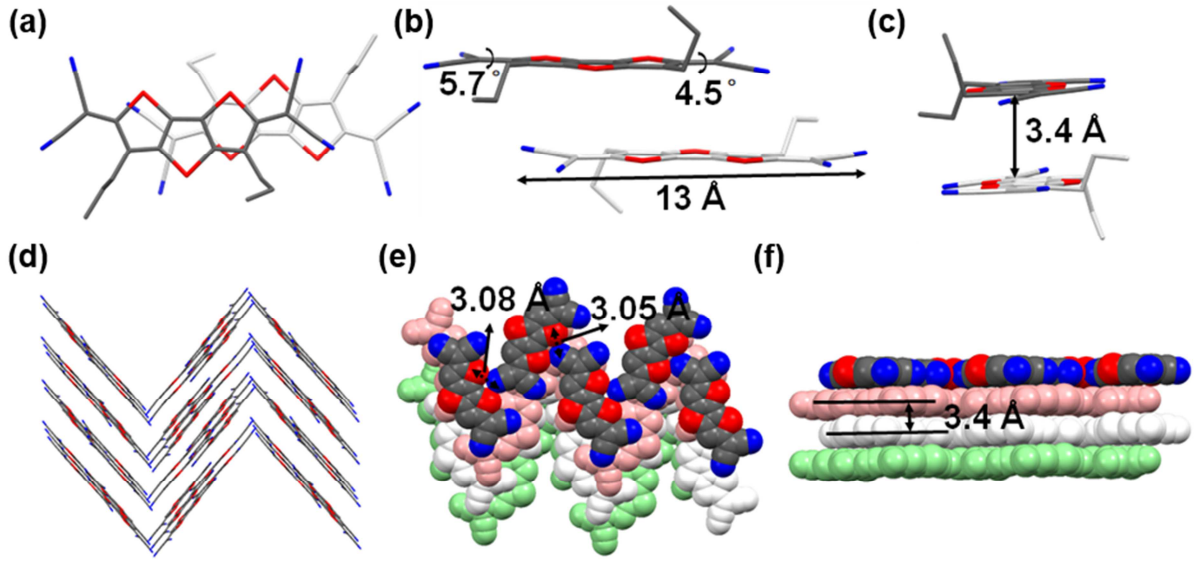

Fig. 5. Single crystal structure of **DTTRQ-3** (all hydrogen atoms have been omitted for clarity). Red and black colors indicate sulfur and carbon atoms, respectively. (a) Top view of two **DTTRQ-3** stacking molecules, (b) Front view of two stacking **DTTRQ-3**, (c) Side view; inter planar distance of 3.4 Å. (d) Slipped 1D stacking, (e) Top view of the zig-zag packing arrangement of **DTTRQ-3** molecules with the intermolecular S-N distances of 3.08 Å and 3.05 Å, and (f) Front view of the zig-zag packing arrangement of **DTTRQ-3** molecules with interlayer distance of 3.40 Å.

3. 4. Thin-film transistor characterization.

The thin films of **SBT** derivatives were characterized as active layers for TFTs and complementary-like inverters. The OTFTs were fabricated with a top-contact/bottom-gate (TC/BG) structure. The surface of the Si/SiO_2 (300 nm) gate dielectric was treated with a PS brush.[85] The organic layers were formed by the solution shearing method to make the highly ordered and anisotropic crystalline structure [86-88]. The gold electrodes were thermally evaporated on the organic layer with various channel widths and lengths. The series of **SBT** materials exhibited p-type characteristics, and their electrical performances are summarized in **Table 2** and **Fig. S5**. These results clearly show the effects of side chain engineering on the SBT core. Although **SBT-14** exhibited decent hole mobility (up to 0.30 $cm^2 V^{-1}s^{-1}$), other

SBT derivatives with different lengths of alkyl substituents showed much lower device performance, with a hole mobility of 10^{-4} – 10^{-2} $cm^2 V^{-1}s^{-1}$.

Table 2
TFT Device Performance Parameters based on the Thin Films of SBT Derivatives.[a] (μ: carrier mobility, I_{on}/I_{off}: current on/off ratio, V_T; threshold voltage).

Compound	Method	Surface treatment	μ^{max} (μ^{avg}) ($cm^2 V^{-1}s^{-1}$)	I_{on}/I_{off}	V_T (V)
SBT-10	SS	PS-brush	0.025 (0.019±0.003)	(19±7.7) × 10^3	-8±1.2
SBT-12			0.0010 (0.0008±0.0002)	(54±6.5) × 10^3	-16±3.3
SBT-14			0.30 (0.26±0.03)	(20±4.8) × 10^2	-39±5.6
SBT-16			0.00053 (0.00045±0.00005)	(29±5.2) × 10^3	-3±1.7
SBT-18			0.0020 (0.0017±0.0003)	(56±6.3) × 10^3	-29±4.3

[a] Measured in ambient and exhibited p-channel characteristics. Maximum and average value among multiple (>10) device measurements.

The BHJ OTFTs were fabricated based on blended films of **SBT-14** (as p-channel semiconductor), the highest performing SBT derivative in this study, and quinoidal **DTTRQ**s (as an n-channel semiconductor) in identical solvent [84]. Four different kinds of **DTTRQ**s with different alkyl side chains were tested to find the effects of side chains of quinoidal **DTTRQ**s on the BHJ transistor performance. The electrical performances of the BHJ OTFTs are summarized in **Table 3**, and the representative transfer and output curves are shown in **Fig. 6** and **S6.** It can be seen that the BHJ OTFTs based on **SBT-14** and **DTTRQ**s showed ambipolar characteristics that were stable in ambient conditions. The device performance of the ambipolar transistors was optimized by varying the blend ratio of **SBT-14** and **DTTRQ**s (**Tables S3** – **S5**). The optimized devices based on **SBT-14** and **DTTRQ (C11)** showed air-stable ambipolar charge transport behaviour with balanced electron and hole mobilities as

high as 0.70 and 0.21 $cm^2 V^{-1}s^{-1}$, respectively (**Table 3**). Note that this result is, to the best of our knowledge, one of the highest balanced ambipolar characteristics for solution-processed small molecules reported to date. The ambipolar transistor exhibited diode-like output curves which is due to the presence of both types of carriers in the active channel layer.[40] The highly positive threshold voltage for the n-type performance and/or the negative threshold voltage for the p-type operation imply electron and hole trapping at the phase-separated interface of the two types of organic materials [89]. The BHJ transistors with other **DTTRQ**s showed relatively lower device performance, with electron and hole mobilities of 0.021– 0.21 and 0.075 – 0.11 $cm^2 V^{-1}s^{-1}$, respectively. For comparison, the other SBT derivatives were also blended with the four DTTRQs, and the results are summarized in **Table S6** with the representative transfer curves in **Figs. S8 – S11.** Due to the poor p-channel characteristics compared with **SBT-14**, the blended films yielded relatively poor ambipolar performance (Table S6).

Table 3
Electrical Performance of the Bulk Heterojunction Ambipolar Thin Film Transistors based on Blend Films of **SBT-14** and Four Different **DTTRQ**s.[a]

Compound (P type)	Compound (N type)	P -channel			N-channel		
		μ_h^{max} (μ_h^{avg}) ($cm^2 V^{-1}s^{-1}$)	V_T (V)	I_{on}/I_{off}	μ_e^{max} (μ_e^{avg}) ($cm^2 V^{-1}s^{-1}$)	V_T (V)	I_{on}/I_{off}
SBT-14	**DTTRQ (C3)**	0.075 (0.069±0.004)	-35 ±4.4	(12±3.1) $\times 10^0$	0.021 (0.017±0.004)	-34 ±5.6	(5.9±2.2) $\times 10^0$
	DTTRQ (C6)	0.11 (0.08±0.02)	-57 ±7.1	(10±2.3) $\times 10^0$	0.21 (0.18±0.03)	9.2 ±1.4	(4.4±3.6) $\times 10^6$
	DTTRQ (C11)	0.21 (0.19±0.02)	-29 ±3.8	(10±3.2) $\times 10^0$	0.70 (0.66±0.02)	25 ±1.5	(5.2±2.9) $\times 10^1$
	DTTRQ (C15)	0.097 (0.095±0.002)	-7.5 ±2.1	(11±5.8) $\times 10^0$	0.055 (0.052±0.001)	-7.6 ±2.7	(10±4.8) $\times 10^0$

[a] Measured in ambient and exhibited ambipolar characteristics. Maximum and average value among multiple (>10) device measurements.

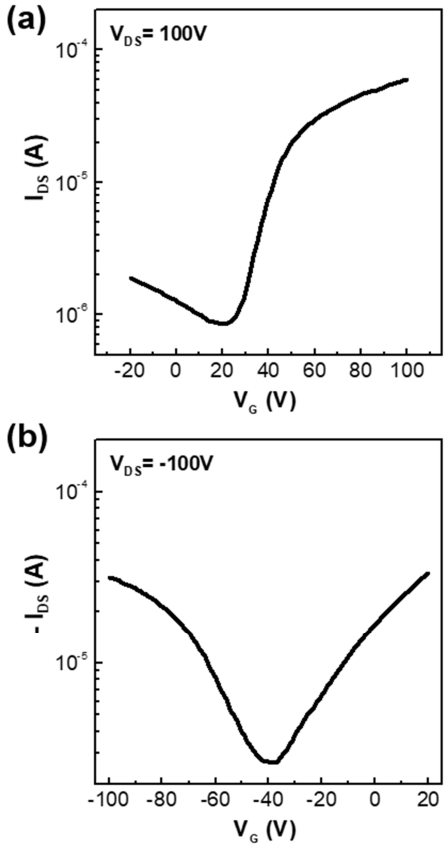

Fig. 6. (a) N-channel and (b) P–channel transfer characteristics of BHJ ambipolar transistors based on blends of **SBT-14** and **DTTRQ (C11)**. Channel widths and lengths of 1000 μm and 100 μm were used, respectively.

The BHJ ambipolar transistors described herein are suitable for the fabrication of high-performance inverters, the building blocks of integrated circuits. Therefore, we have fabricated complementary-like inverters employing two identical ambipolar transistors, and the transfer characteristics of the inverters are shown in **Fig. 7**. Because of its unique ambipolar characteristics, the inverter was capable of operating in both positive and negative V_{IN} and V_{DD}. The performance of complementary-like inverters can usually be demonstrated by the transfer gain, as defined as dV_{OUT}/dV_{IN}, where V_{OUT} and V_{IN} are the output and input voltages, respectively. We calculated the transfer gains of the inverter at two different supply voltages (V_{DD}) of -100 V and 100 V. As shown in the results, at negative V_{IN} and V_{DD}, the

inverter showed a high maximum transfer gain of 81, while at positive V_{IN} and V_{DD}, a gain of 40 was obtained.

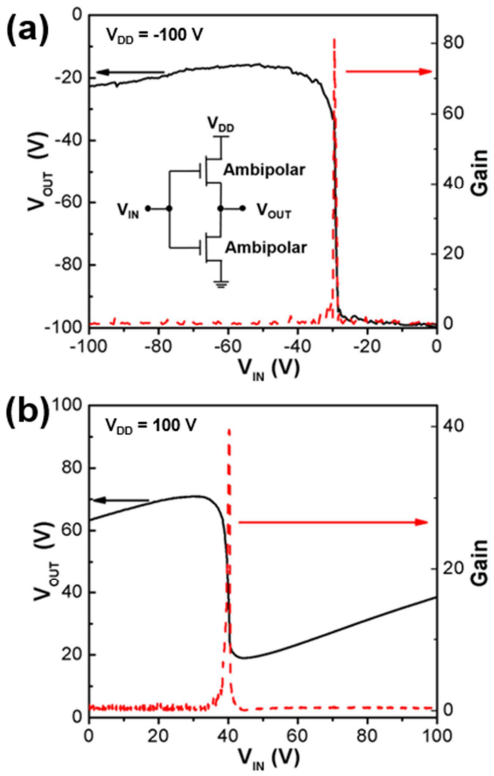

Fig. 7. Voltage transfer characteristics (VTCs) of complementary-like inverters using two identical ambipolar thin-film transistors based on **SBT-14** and **DTTRQ (C11)** in the first (a) and third (b) quadrants with the corresponding voltage gain. The inset shows the circuit diagram, and the plots of gains ($-dV_{OUT}/dV_{IN}$) are given in red.

Thin-film microstructure and morphology

The film microstructure and surface morphology of the new solution-processed semiconductor thin films were characterized using wide-angle θ-2θ X-ray diffraction and atomic force microscopy to evaluate device performance. Conventional θ-2θ XRD scans of thin films were performed to investigate the microstructural order in the semiconductor thin films. As shown in **Figs. S12a** and **S12c**, thin films of **SBT-10** and **SBT-14** showed multiple

Bragg reflections with diffraction peaks up to the fifth- and sixth-order, respectively, suggesting the highly crystalline microstructure of the corresponding thin films. **SBT-12** did not exhibit any significant Bragg reflections, indicating poor film texture (**Fig. S12b**), while **SBT-16**, and **SBT-18** showed relatively broad peaks with smaller intensities (**Figs. S12d, e**). The film of **SBT-10**, **SBT-12**, **SBT-14**, **SBT-16**, and **SBT-18** exhibited (001) diffraction peaks at 2θ = 5.58, 4.92, 4.80, 4.34, and 4.1, corresponding to d-spacing of 15.8, 17.9, 18.4, 20.7 and 21.5 angstrom, respectively. As shown in the results, **SBT**s with a longer side chain length afforded larger *d*-spacings. The surface morphologies of **SBT** derivatives were characterized by AFM (**Fig. S13**). Overall, solution-sheared films of **SBT** derivatives exhibited microscale terrace-like morphologies along the shearing direction, with scattered small aggregates. In particular, films of **SBT-14** showed a relatively smooth surface with a root-mean-square (RMS) surface roughness of 0.82 nm, while films of other **SBT** derivatives showed an RMS roughness of 1.21 – 7.69 nm (**Fig. S13**). Note that high film texture and relatively smooth film morphology with good interconnectivity of **SBT-14** could afford better electrical performance of the corresponding films, compared to other **SBT** derivatives (vide supra). It can also be implied that the different lengths of the alkyl chains in the semiconducting molecule affect the overall film morphology [90].

Wide-angle θ-2θ XRD and AFM were also used to characterize the BHJ blend films of **SBT-14** and **DTTRQs**. The XRD results are shown in **Fig. 8** and **S14 – S18**. It can be seen that all the BHJ films of **SBT-14** and **DTTRQ** exhibited two sets of Bragg reflections up to the sixth peaks. Two sets of reflections for all blend films correspond to the primary peak of the single component films (**SBT-14** and **DTTRQ**s), which indicates that BHJ films are phase-separated (**Fig. 8**) [78]. In particular, the primary XRD peaks for each component for blend films of **SBT-14:DTTRQ(C11)** were investigated in more detail, as shown in **Fig. 8B**.

It can be seen that the relative intensity of the primary peak for **SBT-14** increased, as the blending ratio of **SBT-14:DTTRQ(C11)** changed from 1:2 to 2:1. This microstructural trend matches well with the corresponding device performance, where BHJ ambipolar transistors showed more of the p-channel characteristic as the content of **SBT-14** increased in the blend film (vide supra, **Table S4**).

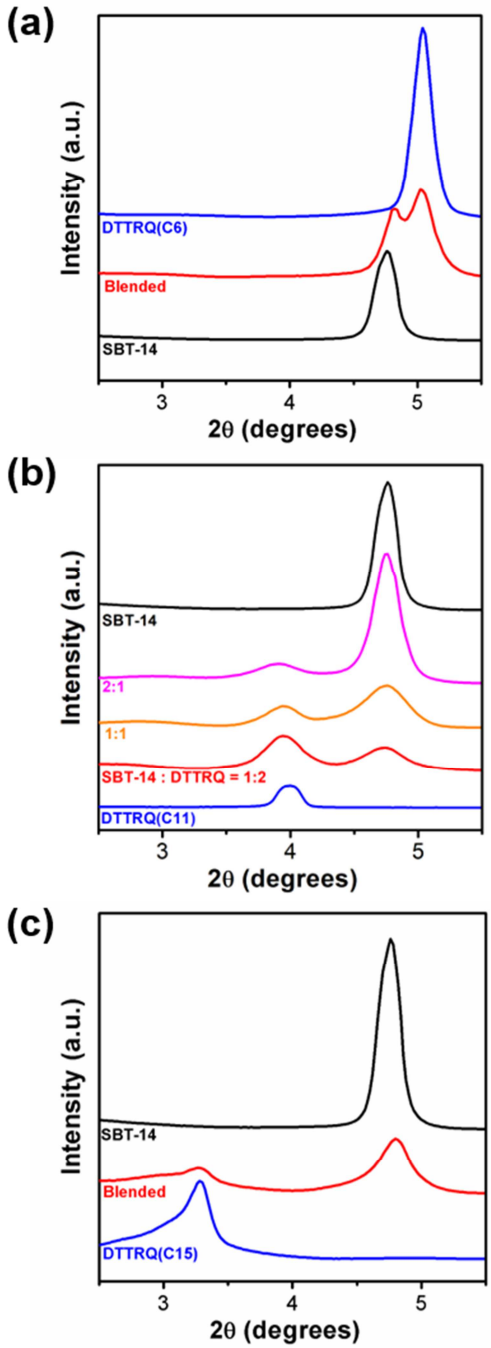

Fig. 8. Wide-angle θ-2θ X-ray diffraction (XRD) scans for blend films of **SBT-14** and (a) **DTTRQ(C6)**, (b) **DTTRQ(C11),** and (c) **DTTRQ(C15)** with different blend ratios, respectively.

Similarly, the surface morphologies of the organic BHJ layers were measured by AFM. As shown in **Fig. 9**, all BHJ films exhibited two distinct phases, a relatively large

terraced region and light regions (as small dots or connected lines). Compared to **Figs. 9a** and **9c** (**SBT-14** with **DTTRQ-6** and **DTTRQ-15**), the light regions in **Fig. 9b** showed relatively better connectivity within a two-phase discontinuous network structure, which might indicate higher/balanced carrier mobilities of the corresponding device (vide supra). Furthermore, the surface morphologies of **SBT-14**/**DTTRQ-11** blend films were measured as a function of blend ratio (**Figs. 9b** and **S19**, **S20**). As the SBT-14 component increased from 1:2 (**Fig. 9b**) to 1:1 (**Fig. S19**) and 2:1 (**Fig. S20**), larger grain sizes were observed with a higher roughness and worse interconnectivity than seen with the optimized blend ratio (**Fig. 9b**). This surface morphology trend matches well with the observed microscopy images (**Fig. S21**).

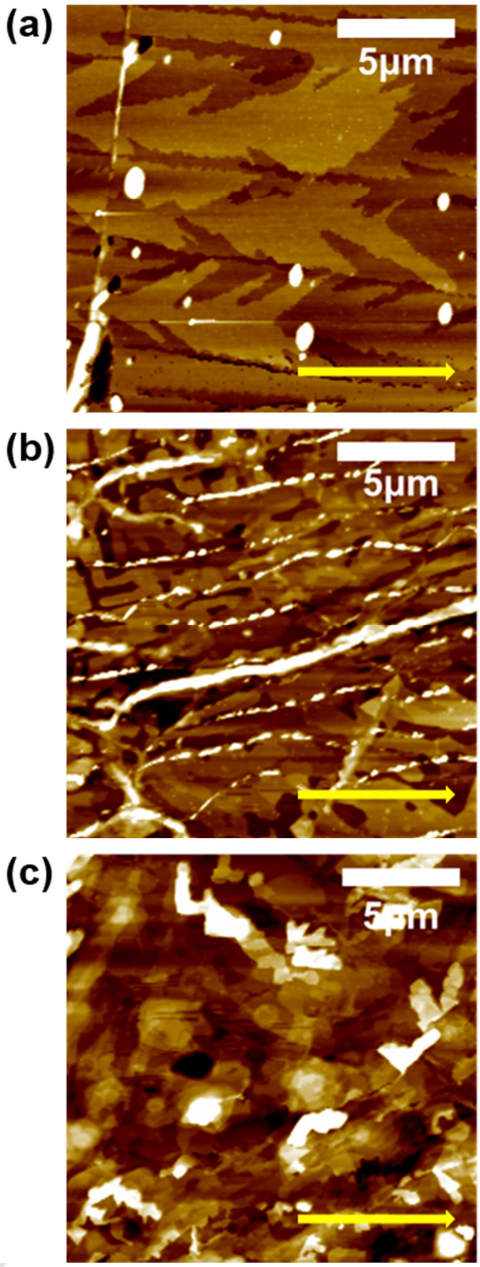

Fig. 9. AFM topographic images for BHJ thin films of **SBT-14** and (a) **DTTRQ(C6)**, (b) **DTTRQ(C11)**, and (c) **DTTRQ(C15)**, respectively. The blending ratio of SBT-14 and DTTRQ(Cn) is 1:2 (Table 3). Scale bar denotes 5 μm and the arrow shows the shearing direction.

4. CONCLUSION

In conclusion, solution-processable thioalkylated bithiophene derivatives with different lengths of side chains have been synthesized and employed as p-channel organic

semiconducting layers for thin-film transistors. The thioalkylated bithiophene derivative with a proper alkyl chain length showed the highest p-channel characteristics. Bulk heterojunction ambipolar transistors were fabricated based on an optimized combination of the highest performing p-channel bithiophene derivative and quinoidal n-channel material, and exhibited high and air-stable performance with well-balanced electron and hole mobilities as high as 0.70 and 0.21 $cm^2 V^{-1} s^{-1}$, respectively. Furthermore, complementary-like inverters fabricated from the ambipolar transistors exhibited high voltage gain of 81. Our work reports one of the highest ambipolar TFT performance based on solution-processable small molecular blends, and demonstrates that the side chain engineering of small molecular organic semiconductors has a significant influence on the electrical performance of TFTs and complementary-like inverters.

Acknowledgements:

This work was supported with grants from the Basic Science Research Program of the National Research Foundation of Korea (NRF-2017R1A2B4001955) funded by the Ministry of Science and ICT, Republic of Korea and the support at National Central University was received from the Ministry of Science and Technology of Taiwan (MOST).

References

[1] Lee J, Chen H-F, Batagoda T, Coburn C, Djurovich PI, Thompson ME, Forrest SR. Deep blue phosphorescent organic light-emitting diodes with very high brightness and efficiency. Nat Mater 2015;15:92.

[2] Mazzio KA, Luscombe CK. The future of organic photovoltaics. Chem Soc Rev

2015;44:78-90.

[3] Zhang C, Chen P, Hu W. Organic Light-Emitting Transistors: Materials, Device Configurations, and Operations. Small 2016;12:1252-1294.

[4] Di C-a, Zhang F, Zhu D. Multi-Functional Integration of Organic Field-Effect Transistors (OFETs): Advances and Perspectives. Adv Mater 2013;25:313-330.

[5] Marshall JL, Uchida K, Frederickson CK, Schütt C, Zeidell AM, Goetz KP, Finn TW, Jarolimek K, Zakharov LN, Risko C, Herges R, Jurchescu OD, Haley MM. Indacenodibenzothiophenes: synthesis, optoelectronic properties and materials applications of molecules with strong antiaromatic character. Chem Sci 2016;7:5547-5558.

[6] Erdmann T, Fabiano S, Milián-Medina B, Hanifi D, Chen Z, Berggren M, Gierschner J, Salleo A, Kiriy A, Voit B, Facchetti A. Naphthalenediimide Polymers with Finely Tuned In-Chain π-Conjugation: Electronic Structure, Film Microstructure, and Charge Transport Properties. Adv Mater 2016;28:9169-9174.

[7] Boopathi KM, Mohan R, Huang T-Y, Budiawan W, Lin M-Y, Lee C-H, Ho K-C, Chu C-W. Synergistic improvements in stability and performance of lead iodide perovskite solar cells incorporating salt additives. J Mater Chem A 2016;4:1591-1597.

[8] Braendlein M, Pappa A-M, Ferro M, Lopresti A, Acquaviva C, Mamessier E, Malliaras GG, Owens RM. Lactate Detection in Tumor Cell Cultures Using Organic Transistor Circuits. Adv Mater 2017;29:1605744.

[9] Hyun WJ, Secor EB, Hersam MC, Frisbie CD, Francis LF. High-Resolution Patterning of Graphene by Screen Printing with a Silicon Stencil for Highly Flexible Printed Electronics. Adv Mater 2015;27:109-115.

[10] Lee S, Reuveny A, Reeder J, Lee S, Jin H, Liu Q, Yokota T, Sekitani T, Isoyama T, Abe Y, Suo Z, Someya T. A transparent bending-insensitive pressure sensor. Nat Nanotech

2016;11:472.

[11] Lüssem B, Keum C-M, Kasemann D, Naab B, Bao Z, Leo K. Doped Organic Transistors. Chem Rev 2016;116:13714-13751.

[12] Marrocchi A, Facchetti A, Lanari D, Santoro S, Vaccaro L. Click-chemistry approaches to π-conjugated polymers for organic electronics applications. Chem Sci 2016;7:6298-6308.

[13] Ozdemir M, Choi D, Kwon G, Zorlu, Y, Kim H, Kim M-G, Seo S, Sen U, Citir M, Kim C, Usta H. Design, synthesis, and characterization of α,ω-disubstituted indeno[1,2-b]fluorene-6,12-dione-thiophene molecular semiconductors. Enhancement of ambipolar charge transport through synthetic tailoring of alkyl substituents. RSC Adv 2016;6;212-226.

[14] Yan H, Chen Z, Zheng Y, Newman C, Quinn JR, Dötz F, Kastler M, Facchetti A. A high-mobility electron-transporting polymer for printed transistors. Nature 2009;457:679.

[15] Tang ML, Mannsfeld SCB, Sun Y-S, Becerril HA, Bao Z. Pentaceno[2,3-b]thiophene, a Hexacene Analogue for Organic Thin Film Transistors. J Am Chem Soc 2009;131:882-883.

[16] Kang B, Kim R, Lee SB, Kwon S-K, Kim Y-H, Cho K. Side-Chain-Induced Rigid Backbone Organization of Polymer Semiconductors through Semifluoroalkyl Side Chains. J Am Chem Soc 2016;138:3679-3686.

[17] Ozdemir R, Choi D, Ozdemir M, Kwon G, Kim H, Sen U, Kim C, Usta H. Ultralow bandgap molecular semiconductors for ambient-stable and solution-processable ambipolar organic field-effect transistors and inverters. J Mater Chem C 2017;5:2368-2379.

[18] Stolte M, Suraru S-L, Diemer P, He T, Burschka C, Zschieschang U, Klauk H, Würthner F. Diketopyrrolopyrrole Organic Thin-Film Transistors: Impact of Alkyl Substituents and Tolerance of Ethylhexyl Stereoisomers. Adv Funct Mater 2016;26:7415-7422.

[19] Schwarze M, Tress W, Beyer B, Gao F, Scholz R, Poelking C, Ortstein K, Günther AA, Kasemann D, Andrienko D, Leo K. Band structure engineering in organic semiconductors. Science 2016;352:1446-1449.

[20] Nielsen CB, Giovannitti A, Sbircea D-T, Bandiello E, Niazi MR, Hanifi DA, Sessolo M, Amassian A, Malliaras GG, Rivnay J, McCulloch I. Molecular design of semiconducting polymers for high-performance organic electrochemical transistors. J Am Chem Soc 2016;138:10252-10259.

[21] Rivnay J. Efficiency through dilution. Nat Mater 2016;15:594.

[22] Di Nuzzo D, Fontanesi C, Jones R, Allard S, Dumsch I, Scherf U, von Hauff E, Schumacher S, Da Como E. How intermolecular geometrical disorder affects the molecular doping of donor–acceptor copolymers. Nat Commun 2015;6:6460.

[23] Ho D, Jeon M, Kim H, Gidron O, Kim C, Seo SY. Solution-processable dithieno[3,2-b:2′,3′-d]thiophene derivatives for organic thin-film transistors and complementary-like inverters. Org Electron 2018;52:356-363.

[24] Melianas A, Pranculis V, Xia Y, Felekidis N, Inganäs O, Gulbinas V, Kemerink M. Photogenerated Carrier Mobility Significantly Exceeds Injected Carrier Mobility in Organic Solar Cells. Adv Energy Mater 2017;7:1602143.

[25] Katz HE, Bao Z, Gilat SL. Synthetic Chemistry for Ultrapure, Processable, and High-Mobility Organic Transistor Semiconductors. Acc Chem Res 2001;34:359-369.

[26] Ozdemir M, Genc S, Ozdemir R, Altintas Y, Citir M, Sen U, Mutlugun E, Usta H. Trans–cis isomerization assisted synthesis of solution-processable yellow fluorescent maleic anhydrides for white-light generation. Synth Met 2015;210:192-200.

[27] Yi W, Zhao S, Sun H, Kan Y, Shi J, Wan S, Li C, Wang H. Isomers of organic semiconductors based on dithienothiophenes: the effect of sulphur atoms positions on the

intermolecular interactions and field-effect performances. J Mater Chem C 2015;3:10856-10861.

[28] Richter LJ, DeLongchamp DM, Amassian A. Morphology Development in Solution-Processed Functional Organic Blend Films: An In Situ Viewpoint. Chem Rev 2017;117:6332-6366.

[29] Mukherjee S, Proctor CM, Tumbleston JR, Bazan GC, Nguyen T-Q, Ade H. Importance of Domain Purity and Molecular Packing in Efficient Solution-Processed Small-Molecule Solar Cells. Adv Mater 2015;27:1105-1111.

[30] Kim H, Reddy MR, Kim H, Choi D, Kim C, Seo SY. Benzothiadiazole- Based Small- Molecule Semiconductors for Organic Thin- Film Transistors and Complementary-like Inverters. Chempluschem 2017;82;742-749.

[31] Chase DT, Fix AG, Kang SJ, Rose BD, Weber CD, Zhong Y, Zakharov LN, Lonergan MC, Nuckolls C, Haley MM. 6,12-Diarylindeno[1,2-b]fluorenes: Syntheses, Photophysics, and Ambipolar OFETs. J Am Chem Soc 2012;134:10349-10352.

[32] Mei J, Diao Y, Appleton AL, Fang L, Bao Z. Integrated Materials Design of Organic Semiconductors for Field-Effect Transistors. J Am Chem Soc 2013;135:6724-6746.

[33] Usta H, Newman C, Chen Z, Facchetti A. Dithienocoronenediimide-Based Copolymers as Novel Ambipolar Semiconductors for Organic Thin-Film Transistors. Adv Mater 2012;24:3678-3684.

[34] Mamillapalli NC, Vegiraju S, Priyanka P, Lin C-Y, Luo X-L, Tsai H-C, Hong S-H, Ni J-S, Lien W-C, Kwon G, Yau SL, Kim C, Liu C-L, Chen M-C. Solution-processable end-functionalized tetrathienoacene semiconductors: Synthesis, characterization and organic field effect transistors applications. Dyes and Pigments 2017;145:584-590.

[35] Ozdemir M, Choi D, Kwon G, Zorlu Y, Cosut B, Kim H, Facchetti A, Kim C, Usta H.

Solution-Processable BODIPY-Based Small Molecules for Semiconducting Microfibers in Organic Thin-Film Transistors. ACS Appl Mater Interfaces 2016;8:14077-14087.

[36] Lim B, Sun H, Noh Y-Y. Highly soluble small-molecule organic semiconductor with trihexylsilyloxy side chain for high-performance organic field-effect transistors with mobility of up to 3.10 cm2 V−1 s−1. Dyes and Pigments 2017;142:17-23.

[37] Huang P-Y, Chen L-H, Chen Y-Y, Chang W-J, Wang J-J, Lii K-H, Yan J-Y, Ho J-C, Lee C-C, Kim C, Chen M-C. Enhanced Performance of Benzothieno[3,2-b]thiophene (BTT)-Based Bottom-Contact Thin-Film Transistors. Chem Eur J 2013;19:3721-3728.

[38] Huang P-Y, Chen L-H, Kim C, Chang H-C, Liang Y-j, Feng C-Y, Yeh C-M, Ho J-C, Lee C-C, Chen M-C. High-Performance Bottom-Contact Organic Thin-Film Transistors Based on Benzo[d,d′]thieno[3,2-b;4,5-b′]dithiophenes (BTDTs) Derivatives. ACS Appl Mater Interfaces 2012;4:6992-6998.

[39] Zhou N, Prabakaran K, Lee B, Chang SH, Harutyunyan B, Guo P, Butler MR, Timalsina A, Bedzyk MJ, Ratner MA, Vegiraju S, Yau S, Wu C-G, Chang RPH, Facchetti A, Chen M-C, Marks TJ. Metal-Free Tetrathienoacene Sensitizers for High-Performance Dye-Sensitized Solar Cells. J Am Chem Soc 2015;137:4414-4423.

[40] Cheng S-S, Huang P-Y, Ramesh M, Chang H-C, Chen L-M, Yeh C-M, Fung C-L, Wu M-C, Liu C-C, Kim C, Lin H-C, Chen M-C, Chu C-W. Solution-Processed Small-Molecule Bulk Heterojunction Ambipolar Transistors. Adv Funct Mater 2014;24:2057-2063.

[41] Zhou N, Vegiraju S, Yu X, Manley EF, Butler MR, Leonardi MJ, Guo P, Zhao W, Hu Y, Prabakaran K, Chang RPH, Ratner MA, Chen LX, Facchetti A, Chen M-C, Marks TJ. Diketopyrrolopyrrole (DPP) functionalized tetrathienothiophene (TTA) small molecules for organic thin film transistors and photovoltaic cells. J Mater Chem C 2015;3:8932-8941.

[42] Xiao K, Liu Y, Qi T, Zhang W, Wang F, Gao J, Qiu W, Ma Y, Cui G, Chen S, Zhan X,

Yu G, Qin J, Hu W, Zhu D. A Highly π-Stacked Organic Semiconductor for Field-Effect Transistors Based on Linearly Condensed Pentathienoacene. J Am Chem Soc 2005;127:13281-13286.

[43] Youn J, Huang P-Y, Huang Y-W, Chen M-C, Lin Y-J, Huang H, Ortiz RP, Stern C, Chung M-C, Feng C-Y, Chen L-H, Facchetti A, Marks TJ. Versatile α,ω-Disubstituted Tetrathienoacene Semiconductors for High Performance Organic Thin-Film Transistors. Adv Funct Mater 2012;22:48-60.

[44] Youn J, Vegiraju S, Emery JD, Leever BJ, Kewalramani S, Lou SJ, Zhang S, Prabakaran K, Ezhumalai Y, Kim C, Huang P-Y, Stern C, Chang W-C, Bedzyk MJ, Chen LX, Chen M-C, Facchetti A, Marks TJ. Diperfluorophenyl Fused Thiophene Semiconductors for n-Type Organic Thin Film Transistors (OTFTs). Adv Electon Mater 2015;1:1500098.

[45] Jones AOF, Chattopadhyay B, Geerts YH, Resel R. Substrate-Induced and Thin-Film Phases: Polymorphism of Organic Materials on Surfaces. Adv Funct Mater 2016;26:2233-2255.

[46] Tsutsui Y, Schweicher G, Chattopadhyay B, Sakurai T, Arlin J-B, Ruzié C, Aliev A, Ciesielski A, Colella S, Kennedy AR, Lemaur V, Olivier Y, Hadji R, Sanguinet L, Castet F, Osella S, Dudenko D, Beljonne D, Cornil J, Samorì P, Seki S, Geerts YH. Unraveling Unprecedented Charge Carrier Mobility through Structure Property Relationship of Four Isomers of Didodecyl[1]benzothieno[3,2-b][1]benzothiophene. Adv Mater 2016;28:7106-7114.

[47] Himmelberger S, Duong DT, Northrup JE, Rivnay J, Koch FPV, Beckingham BS, Stingelin N, Segalman RA, Mannsfeld SCB, Salleo A. Role of Side-Chain Branching on Thin-Film Structure and Electronic Properties of Polythiophenes. Adv Funct Mater 2015;25:2616-2624.

[48] Glaudell AM, Cochran JE, Patel SN, Chabinyc ML. Impact of the Doping Method on Conductivity and Thermopower in Semiconducting Polythiophenes. Adv Energy Mater 2015;5:1401072.

[49] Mitsui C, Tsuyama H, Shikata R, Murata Y, Kuniyasu H, Yamagishi M, Ishii H, Yamamoto A, Hirose Y, Yano M, Takehara T, Suzuki T, Sato H, Yamano A, Fukuzaki E, Watanabe T, Usami Y, Takeya J, Okamoto T. High performance solution-crystallized thin-film transistors based on V-shaped thieno[3,2-f:4,5-f′]bis[1]benzothiophene semiconductors. J Mater Chem C 2017;5:1903-1909.

[50] Zhang W, Han Y, Zhu X, Fei Z, Feng Y, Treat ND, Faber H, Stingelin N, McCulloch I, Anthopoulos TD, Heeney M. A Novel Alkylated Indacenodithieno[3,2-b]thiophene-Based Polymer for High-Performance Field-Effect Transistors. Adv Mater 2016;28:3922-3927.

[51] Zhou K, Dong H, Zhang H-l, Hu W. High performance n-type and ambipolar small organic semiconductors for organic thin film transistors. Phys Chem Chem Phys 2014;16:22448-22457.

[52] Zhao Y, Guo Y, Liu Y. 25th Anniversary Article: Recent Advances in n-Type and Ambipolar Organic Field-Effect Transistors. Adv Mater 2013;25:5372-5391.

[53] Ozdemir R, Choi D, Ozdemir M, Kwon G, Kim H, Sen U, Kim C, Usta H. Ultralow bandgap molecular semiconductors for ambient-stable and solution-processable ambipolar organic field-effect transistors and inverters. J Mater Chem C 2017;5:2368-2379.

[54] Kim FS, Guo X, Watson MD, Jenekhe SA. High-mobility Ambipolar Transistors and High-gain Inverters from a Donor–Acceptor Copolymer Semiconductor. Adv Mater 2010;22:478-482.

[55] Meijer EJ, de Leeuw DM, Setayesh S, van Veenendaal E, Huisman BH, Blom PWM, Hummelen JC, Scherf U, Klapwijk TM. Solution-processed ambipolar organic field-effect

transistors and inverters. Nat Mater 2003;2:678.

[56] Kim B, Geier ML, Hersam MC, Dodabalapur A. Inkjet printed circuits based on ambipolar and p-type carbon nanotube thin-film transistors. Sci Rep 2017;7:39627.

[57] Chin XY, Pace G, Soci C, Caironi M. Ambipolar charge distribution in donor–acceptor polymer field-effect transistors. J Mater Chem C 2017;5:754-762.

[58] Bucella SG, Salazar-Rios JM, Derenskyi V, Fritsch M, Scherf U, Loi MA, Caironi M. Inkjet Printed Single-Walled Carbon Nanotube Based Ambipolar and Unipolar Transistors for High-Performance Complementary Logic Circuits. Adv Electon Mater 2016;2:1600094.

[59] Liang Z, Tang Q, Mao R, Liu D, Xu J, Miao Q. The Position of Nitrogen in N-Heteropentacenes Matters. Adv Mater 2011;23:5514-5518.

[60] Tang ML, Reichardt AD, Miyaki N, Stoltenberg RM, Bao Z. Ambipolar, High Performance, Acene-Based Organic Thin Film Transistors. J Am Chem Soc 2008;130:6064-6065.

[61] Tang ML, Oh JH, Reichardt AD, Bao Z. Chlorination: A General Route toward Electron Transport in Organic Semiconductors. J Am Chem Soc 2009;131:3733-3740.

[62] Cornil J, Brédas J-L, Zaumseil J, Sirringhaus H. Ambipolar Transport in Organic Conjugated Materials. Adv Mater 2007;19:1791-1799.

[63] Ortiz RP, Herrera H, Seoane C, Segura JL, Facchetti A, Marks TJ. Rational Design of Ambipolar Organic Semiconductors: Is Core Planarity Central to Ambipolarity in Thiophene–Naphthalene Semiconductors? Chem Eur J 2012;18:532-543.

[64] Riaño A, Mayorga Burrezo P, Mancheño MJ, Timalsina A, Smith J, Facchetti A, Marks TJ, López Navarrete JT, Segura JL, Casado J, Ponce Ortiz R. The unusual electronic structure of ambipolar dicyanovinyl-substituted diketopyrrolopyrrole derivatives. J Mater Chem C 2014;2:6376-6386.

[65] Meager I, Nikolka M, Schroeder BC, Nielsen CB, Planells M, Bronstein H, Rumer JW, James DI, Ashraf RS, Sadhanala A, Hayoz P, Flores J-C, Sirringhaus H, McCulloch I. Thieno[3,2-b]thiophene Flanked Isoindigo Polymers for High Performance Ambipolar OFET Applications. Adv Funct Mater 2014;24:7109-7115.

[66] Ma T, Jiang K, Chen S, Hu H, Lin H, Li Z, Zhao J, Liu Y, Chang Y-M, Hsiao C-C, Yan H. Efficient Low-Bandgap Polymer Solar Cells with High Open-Circuit Voltage and Good Stability. Adv Energy Mater 2015;5:1501282.

[67] Figà V, Chiappara C, Ferrante F, Casaletto MP, Principato F, Cataldo S, Chen Z, Usta H, Facchetti A, Pignataro B. Symmetric naphthalenediimidequaterthiophenes for electropolymerized electrochromic thin films. J Mater Chem C 2015;3:5985-5994.

[68] Kim J, Han AR, Hong J, Kim G, Lee J, Shin TJ, Oh JH, Yang C. Ambipolar Semiconducting Polymers with π-Spacer Linked Bis-Benzothiadiazole Blocks as Strong Accepting Units. Chem Mater 2014;26:4933-4942.

[69] Nielsen CB, Turbiez M, McCulloch I. Recent Advances in the Development of Semiconducting DPP-Containing Polymers for Transistor Applications. Adv Mater 2013;25:1859-1880.

[70] Nakano M, Osaka I, Takimiya K. Naphthodithiophene Diimide (NDTI)-Based Semiconducting Copolymers: From Ambipolar to Unipolar n-Type Polymers. Macromolecules 2015;48:576-584.

[71] Lei T, Dou J-H, Ma Z-J, Liu C-J, Wang J-Y, Pei J. Chlorination as a useful method to modulate conjugated polymers: balanced and ambient-stable ambipolar high-performance field-effect transistors and inverters based on chlorinated isoindigo polymers. Chem Sci 2013;4:2447-2452.

[72] Fallahi A, Taromi FA, Mohebbi A, Yuen JD, Shahinpoor M. A novel ambipolar

polymer: from organic thin-film transistors to enhanced air-stable blue light emitting diodes. J Mater Chem C 2014;2:6491-6501.

[73] Gao Y, Zhang X, Tian H, Zhang J, Yan D, Geng Y, Wang F. High Mobility Ambipolar Diketopyrrolopyrrole-Based Conjugated Polymer Synthesized Via Direct Arylation Polycondensation. Adv Mater 2015;27:6753-6759.

[74] Khim D, Cheon YR, Xu Y, Park W-T, Kwon S-K, Noh Y-Y, Kim Y-H. Facile Route To Control the Ambipolar Transport in Semiconducting Polymers. Chem Mater 2016;28:2287-2294.

[75] Gruber M, Jung S-H, Schott S, Venkateshvaran D, Kronemeijer AJ, Andreasen JW, McNeill CR, Wong WWH, Shahid M, Heeney M, Lee J-K, Sirringhaus H. Enabling high-mobility, ambipolar charge-transport in a DPP-benzotriazole copolymer by side-chain engineering. Chem Sci 2015;6:6949-6960.

[76] Chen Z, Lee MJ, Shahid Ashraf R, Gu Y, Albert-Seifried S, Meedom Nielsen M, Schroeder B, Anthopoulos TD, Heeney M, McCulloch I, Sirringhaus H. High-Performance Ambipolar Diketopyrrolopyrrole-Thieno[3,2-b]thiophene Copolymer Field-Effect Transistors with Balanced Hole and Electron Mobilities. Adv Mater 2012;24:647-652.

[77] Smith J, Hamilton R, McCulloch I, Stingelin-Stutzmann N, Heeney M, Bradley DDC, Anthopoulos TD. Solution-processed organic transistors based on semiconducting blends. J Mater Chem 2010;20:2562-2574.

[78] Xu X, Xiao T, Gu X, Yang X, Kershaw SV, Zhao N, Xu J, Miao Q. Solution-Processed Ambipolar Organic Thin-Film Transistors by Blending p- and n-Type Semiconductors: Solid Solution versus Microphase Separation. ACS Appl Mater Interfaces 2015;7:28019-28026.

[79] Ho D, Jeon M, Kim H, Gidron O, Kim C, Seo S. Solution-processable dithieno[3,2-

b:2′,3′-d]thiophene derivatives for organic thin-film transistors and complementary-like inverters. Org Electron 2018;52:356-363.

[80] Laquai F, Andrienko D, Mauer R, Blom PWM. Charge Carrier Transport and Photogeneration in P3HT:PCBM Photovoltaic Blends. Macromol Rapid Commun 2015;36:1001-1025.

[81] Heiber MC, Kister K, Baumann A, Dyakonov V, Deibel C, Nguyen T-Q. Impact of Tortuosity on Charge-Carrier Transport in Organic Bulk Heterojunction Blends. Phys Rev Applied 2017;8:054043.

[82] Chen X, Zhang G, Luo H, Li Y, Liu Z, Zhang D. Ambipolar charge-transport property for the D–A complex with naphthalene diimide motif. J Mater Chem C 2014;2:2869-2876.

[83] Qin Y, Zhang J, Zheng X, Geng H, Zhao G, Xu W, Hu W, Shuai Z, Zhu D. Charge-Transfer Complex Crystal Based on Extended-π-Conjugated Acceptor and Sulfur-Bridged Annulene: Charge-Transfer Interaction and Remarkable High Ambipolar Transport Characteristics. Adv Mater 2014;26:4093-4099.

[84] Vegiraju S, He G-Y, Kim C, Priyanka P, Chiu Y-J, Liu C-W, Huang C-Y, Ni J-S, Wu Y-W, Chen Z, Lee G-H, Tung S-H, Liu C-L, Chen M-C, Facchetti A. Solution-Processable Dithienothiophenoquinoid (DTTQ) Structures for Ambient-Stable n-Channel Organic Field Effect Transistors. Adv Funct Mater 2017;27:1606761.

[85] DiBenedetto SA, Facchetti A, Ratner MA, Marks TJ. Molecular Self-Assembled Monolayers and Multilayers for Organic and Unconventional Inorganic Thin-Film Transistor Applications. Adv Mater 2009;21:1407-1433.

[86] Becerril HA, Roberts ME, Liu Z, Locklin J, Bao Z. High-Performance Organic Thin-Film Transistors through Solution-Sheared Deposition of Small-Molecule Organic

Semiconductors. Adv Mater 2008;20:2588-2594.

[87] Giri G, Verploegen E, Mannsfeld SCB, Atahan-Evrenk S, Kim DH, Lee SY, Becerril HA, Aspuru-Guzik A, Toney MF, Bao Z. Tuning charge transport in solution-sheared organic semiconductors using lattice strain. Nature 2011;480:504.

[88] Diao Y, Tee BCK, Giri G, Xu J, Kim DH, Becerril HA, Stoltenberg RM, Lee TH, Xue G, Mannsfeld SCB, Bao Z. Solution coating of large-area organic semiconductor thin films with aligned single-crystalline domains. Nat Mater 2013;12:665.

[89] High-performance organic thin-film transistors with metal oxide/metal bilayer electrode. Appl Phys Lett 2005;87:193508.

[90] Chen J, Subramanian S, Parkin SR, Siegler M, Gallup K, Haughn C, Martin DC, Anthony JE. The influence of side chains on the structures and properties of functionalized pentacenes. J Mater Chem 2008;18:1961-1969.

[91] Vegiraju S, Chang B-C, Priyanka P, Huang D-Y, Wu K-Y, Li L-H, Chang W-C, Lai Y-Y, Hong S-H, Yu B-C, Wang C-L, Chang W-J, Liu C-L, Chen M-C, Facchetti A. Intramolecular Locked Dithioalkylbithiophene-Based Semiconductors for High-Performance Organic Field-Effect Transistors. Adv Mater 2017;29:1702414.

[92] Park SH, Lee HS, Kim J-D, Breiby DW, Kim E, Park YD, Ryu DY, Lee DR, Cho JH. A polymer brush organic interlayer improves the overlying pentacene nanostructure and organic field-effect transistor performance. J Mater Chem 2011;21:15580-15586.

SUPPORTING INFORMATION

Solution-processable small molecules for bulk heterojunction ambipolar thin-film transistors and complementary-like inverters

Dongil Ho,[a,1] Sureshraju Vegiraju,[b,1] Donghee Choi,[a] Chang-Hui Cho,[b] Guhyun Kwon,[a] Po-Chun Huang,[b] Gene-Hsiang Lee,[c] Taeshik Earmme,[d] Shueh Lin Yau,[b] Ming-Chou Chen,*[,b] and Choongik Kim*[,a]

[a] D. Ho, D. Choi, G. Kwon, Prof. C. Kim,

Department of Chemical and Biomolecular Engineering, Sogang University, Mapo-gu, Seoul, 04107 Republic of Korea

E-mail: choongik@sogang.ac.kr

[b] Dr. S. Vegiraju,+ Prof. M.-C. Chen, C.-H. Cho, P.-C. Huang, Prof. S. L. Yau

Department of Chemistry and Research Center of New Generation Light Driven Photovoltaic Modules,, National Central University, Taoyuan, 32001 Taiwan

E-mail: mcchen@cc.ncu.edu.tw

[c] Dr. G.-H. Lee

Instrumentation Center National Taiwan University Taipei 10617, Taiwan

[d] Prof. T. Earmme

Department of Chemical Engineering, Hongik University, Mapo-gu, Seoul, 04066 Republic of Korea.

[1] These authors contributed equally to this work.

Keywords: organic thin-film transistors; organic semiconductor; bithiophene; bulk heterojunction transistors; CMOS inverter

Contents

18 (i, j) employed in this study. (Measured in ambient and exhibited p-channel characteristics).

12. **Fig. S6.** (a) N type output curve (b) P type output curve of BHJ ambipolar transistors based on blends of **SBT-14** and **DTTRQ (C11)**.

13. **Fig. S7.** (Top) N-channel and (Bottom) P–channel transfer characteristics of BHJ ambipolar transistors based on blends of **SBT-14** and (a) **DTTRQ (C3)**, (b) **DTTRQ (C6)**, and (c) **DTTRQ (C15)**.

14. **Fig. S8.** (Top) N-channel and (Bottom) P–channel transfer characteristics of BHJ ambipolar transistors based on blends of **SBT-10** and (a) **DTTRQ (C3)**, (b) **DTTRQ (C6)**, (c) **DTTRQ (C11)**, and (d) **DTTRQ (C15)**.

15. **Fig. S9.** (Top) N-channel and (Bottom) P–channel transfer characteristics of BHJ ambipolar transistors based on blends of **SBT-12** and (a) **DTTRQ (C3)**, (b) **DTTRQ (C6)**, (c) **DTTRQ (C11)**, and (d) **DTTRQ (C15)**.

16. **Fig. S10.** (Top) N-channel and (Bottom) P–channel transfer characteristics of BHJ ambipolar transistors based on blends of **SBT-16** and (a) **DTTRQ (C3)**, (b) **DTTRQ (C6)**, (c) **DTTRQ (C11)**, and (d) **DTTRQ (C15)**.

17. **Fig. S11.** (Top) N-channel and (Bottom) P–channel transfer characteristics of BHJ ambipolar transistors based on blends of **SBT-18** and (a) **DTTRQ (C3)**, (b) **DTTRQ (C6)**, (c) **DTTRQ (C11)**, and (d) **DTTRQ (C15)**.

18. **Fig. S12.** θ-2θ X-ray diffraction (XRD) scans of solution-sheared thin films of **SBT-10** (a), **SBT-12** (b), **SBT-14** (c), **SBT-16** (d), and **SBT-18** (e).

19. **Fig. S13.** Solution-sheared thin-film AFM topographic image of **SBT-10** (a), **SBT-12** (b), **SBT-14** (c), **SBT-16** (d), and **SBT-18** (e). Scale bar denotes 2 μm and the arrow shows the shearing direction.

20. **Fig. S14.** *θ*-2*θ* X-ray diffraction (XRD) scans of BHJ thin film of **SBT-14:DTTRQ(C6) = 1:2**.

21. **Fig. S15.** *θ*-2*θ* X-ray diffraction (XRD) scans of BHJ thin film of **SBT-14:DTTRQ(C11) = 1:2**.

22. **Fig. S16.** *θ*-2*θ* X-ray diffraction (XRD) scans of BHJ thin film of **SBT-14:DTTRQ(C11) = 1:1**.

23. **Fig. S17.** *θ*-2*θ* X-ray diffraction (XRD) scans of BHJ thin film of **SBT-14:DTTRQ(C11) = 2:1**.

24. **Fig. S18.** *θ*-2*θ* X-ray diffraction (XRD) scans of BHJ thin film of **SBT-14:DTTRQ(C15) = 1:2**.

25. **Fig. S19.** BHJ thin-film AFM topographic image of **SBT-14**:**DTTRQ(C11)** = 1:1. Scale bar denotes 2 μm and the arrow shows the shearing direction.

26. **Fig. S20.** BHJ thin-film AFM topographic image of **SBT-14**:**DTTRQ(C11)** = 2:1. Scale bar denotes 2 μm and the arrow shows the shearing direction.

27. **Fig. S21.** Microscopy images for BHJ thin-film of **SBT-14**:**DTTRQ(C11)** = 1:2 (a), 1:1 (b), 2:1 (c). Scale bar denotes 50 μm and the arrow shows the shearing direction.

Table S1. Summary of Crystal Structure Data for **SBT-10**.

Bond precision:	C-C = 0.0025 A		Wavelength=1.54178
Cell:	a=5.2161(2)	b=13.4218(4)	c=15.6551(5)
	alpha=83.8879(11)	beta=88.3815(10)	gamma=81.154(1)
Temperature: 200 K			
	Calculated		Reported
Volume	1076.73(6)		1076.73(6)
Space group	P -1		P -1
Hall group	-P 1		-P 1
Moiety formula	C44 H50 S10		?
Sum formula	C44 H50 S10		C44 H50 S10
Mr	899.44		899.44
Dx,g cm-3	1.387		1.387
Z	1		1
Mu (mm-1)	4.986		4.986
F000	474.0		474.0
F000'	478.13		
h,k,lmax	6,16,19		6,16,19
Nref	4084		4069
Tmin,Tmax	0.651,0.870		0.598,0.753
Tmin'	0.171		
Correction method= # Reported T Limits: Tmin=0.598 Tmax=0.753 AbsCorr = MULTI-SCAN			
Data completeness= 0.996		Theta(max)= 69.997	
R(reflections)= 0.0307(3787)		wR2(reflections)= 0.0862(4069)	
S = 1.052	Npar= 245		

Table S2. Summary of Crystal Structure Data for **DTTRQ-3**.

Bond precision:	C-C = 0.0041 A		Wavelength=0.71073
Cell:	a=14.5992(7)	b=10.4541(4)	c=25.5360(11)
	alpha=90	beta=90	gamma=90
Temperature: 296 K			
	Calculated		Reported
Volume	3897.3(3)		3897.3(3)
Space group	P b c a		Pbca
Hall group	-P 2ac 2ab		?
Moiety formula	C20 H14 N4 S3		?
Sum formula	C20 H14 N4 S3		C20 H14 N4 S3
Mr	406.53		406.53
Dx,g cm-3	1.386		1.386
Z	8		8
Mu (mm-1)	0.393		0.393
F000	1680.0		1680.0
F000'	1683.41		
h,k,lmax	19,14,34		19,13,34
Nref	4907		4872
Tmin,Tmax	0.963,0.977		0.697,0.746
Tmin'	0.946		

Correction method= # Reported T Limits: Tmin=0.697 Tmax=0.746 AbsCorr = MULTI-SCAN

Data completeness= 0.993 Theta(max)= 28.450

R(reflections)= 0.0535(2303) wR2(reflections)= 0.1218(4872)

S = 0.988 Npar= 246

Table S3. Electronic performance of the devices based on three different blending ratios of **SBT-14** and **DTTRQ (C6)**. Each of them was optimized with different solution shearing conditions and measured in ambient.

Blending ratio		**P -channel**			**N-channel**		
SBT-14	**DTTRQ (C6)**	μ_h ($cm^2 V^{-1}s^{-1}$)	V_T (V)	I_{on}/I_{off}	μ_e ($cm^2 V^{-1}s^{-1}$)	V_T (V)	I_{on}/I_{off}
1	**2**	0.11	-51	8.4	0.21	9.9	4.0×10^6
1	**1**	0.00035	-2.0	4.7	0.0010	14	3.7×10^3
2	**1**	0.0031	7.9	3.4×10^1	0.0026	-38	5.4

Table S4. Electronic performance of the devices based on three different blending ratios of **SBT-14** and **DTTRQ (C11)**. Each of them was optimized with different solution shearing conditions and measured in ambient.

Blending ratio		**P -channel**			**N-channel**		
SBT-14	**DTTRQ (C11)**	μ_h ($cm^2 V^{-1}s^{-1}$)	V_T (V)	I_{on}/I_{off}	μ_e ($cm^2 V^{-1}s^{-1}$)	V_T (V)	I_{on}/I_{off}
1	**2**	0.21	-31	1.2×10^1	0.70	24	7.0×10^1
1	**1**	0.0083	-6.0	3.3	0.022	-20	9.9
2	**1**	0.050	4.1	1.3×10^1	0.018	-8.8	5.9

Table S5. Electronic performance of the devices based on three different blending ratios of **SBT-14** and **DTTRQ (C15)**. Each of them was optimized with different solution shearing conditions and measured in ambient.

Blending ratio		**P -channel**			**N-channel**		
SBT-14	**DTTRQ (C15)**	μ_h (cm^2 $V^{-1}s^{-1}$)	V_T (V)	I_{on}/I_{off}	μ_e (cm^2 $V^{-1}s^{-1}$)	V_T (V)	I_{on}/I_{off}
1	**2**	0.013	9.3	7.3	0.055	-8.7	6.4×10^1
1	**1**	0.0097	15	3.9	0.035	-17	2.9×10^1
2	**1**	0.097	-8.9	1.6×10^1	0.0062	-57	2.0

Table S6. Electrical Performance of the Bulk Heterojunction Ambipolar Thin Film Transistors based on Blend Films of Four Different **SBTs** and Four Different **DTTRQ**s.[a]

Compd. (P type)	Compd. (N type)	P -channel			N-channel		
		μ_h^{max} (μ_h^{avg}) ($cm^2 V^{-1}s^{-1}$)[b]	V_T (V)	I_{on}/I_{off}	μ_e^{max} (μ_e^{avg}) ($cm^2 V^{-1}s^{-1}$)[b]	V_T (V)	I_{on}/I_{off}
SBT-10	**DTTRQ (C3)**	-	-	-	0.053 (0.045±0.006)	-19 ±3.2	(5.8±1.1) ×10^2
	DTTRQ (C6)	0.00040 (0.00031±0.00005)	65 ±3.7	(1.6±0.3) ×10^0	0.10 (0.08±0.02)	-15 ±4.6	(1.1±0.8) ×10^2
	DTTRQ (C11)	0.0013 (0.0009±0.0004)	35 ±4.8	(2.5±0.4) ×10^0	0.046 (0.042±0.003)	-7 ±2.8	(2.1±0.4) ×10^1
	DTTRQ (C15)	0.00057 (0.00050±0.00003)	51 ±3.5	(2.4±0.4) ×10^0	0.0022 (0.0020±0.0002)	-32 ±3.4	(8±0.3) ×10^0
SBT-12	**DTTRQ (C3)**	-	-	-	0.067 (0.055±0.004)	-27 ±3.1	(3.8±1.2) ×10^4
	DTTRQ (C6)	-	-	-	0.11 (0.09±0.02)	-12 ±2.4	(9.2±2.3) ×10^4
	DTTRQ (C11)	0.00012 (0.00009±0.00002)	22 ±3.5	(1.2±0.5) ×10^0	0.033 (0.027±0.003)	-4.5 ±0.9	(1.6±0.4) ×10^2
	DTTRQ (C15)	0.000012 (0.00008±0.00002)	63 ±2.8	(1.6±0.3) ×10^0	0.0093 (0.0087±0.0003)	-9.7 ±1.3	(4.1±0.8) ×10^2
SBT-16	**DTTRQ (C3)**	-	-	-	0.15 (0.11±0.04)	-43 ±3.3	(3.6±0.4) ×10^3
	DTTRQ (C6)	-	-	-	0.053 (0.050±0.003)	-16 ±1.8	(6.2±0.7) ×10^2
	DTTRQ (C11)	0.00012 (0.00008±0.00002)	51 ±3.8	(1.7±0.2) ×10^0	0.0015 (0.0012±0.0001)	-73 ±5.7	(6.1±0.5) ×10^0
	DTTRQ (C15)	0.000046 (0.000040±0.000004)	84 ±2.6	(1.6±0.2) ×10^0	0.0052 (0.0049±0.0002)	-34 ±2.5	(3.1±0.6) ×10^1
SBT-18	**DTTRQ (C3)**	-	-	-	0.11 (0.09±0.01)	-13 ±1.8	(1.9±0.8) ×10^4
	DTTRQ (C6)	0.00097 (0.00088±0.00005)	33 ±3.8	(1.4±0.3) ×10^0	0.071 (0.068±0.003)	-21 ±2.6	(3.4±0.2) ×10^1
	DTTRQ (C11)	0.0043 (0.0038±0.0003)	20 ±4.2	(3.6±0.4) ×10^0	0.0038 (0.0034±0.0004)	-87 ±2.3	(2.9±0.5) ×10^0
	DTTRQ (C15)	0.00047 (0.00039±0.00004)	24 ±3.6	(2.9±0.3) ×10^0	0.0010 (0.0008±0.0002)	-155 ±4.4	(2.4±0.6) ×10^0

[a] Measured in ambient and exhibited ambipolar characteristics. [b] Maximum and average mobility value based on multiple (>10) device measurements.

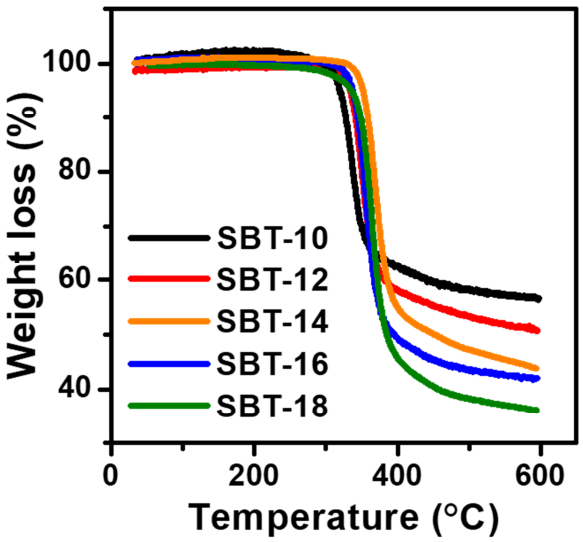

Fig. S1. TGA curves of **SBT-10 – 18**.

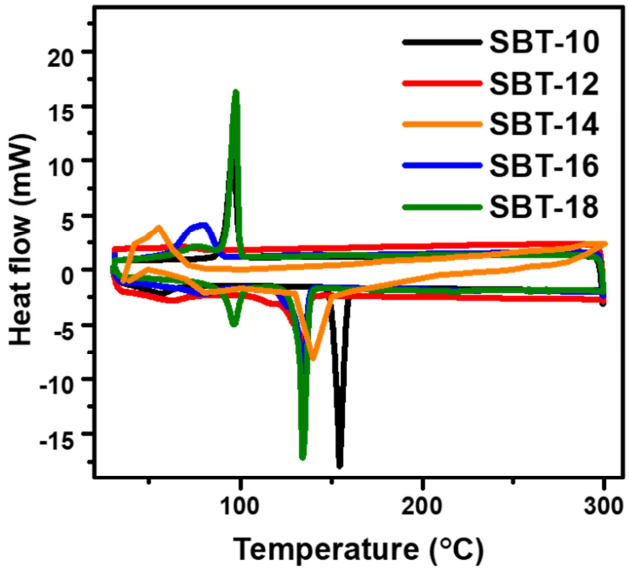

Fig. S2. DSC of **SBT-10 – 18**.

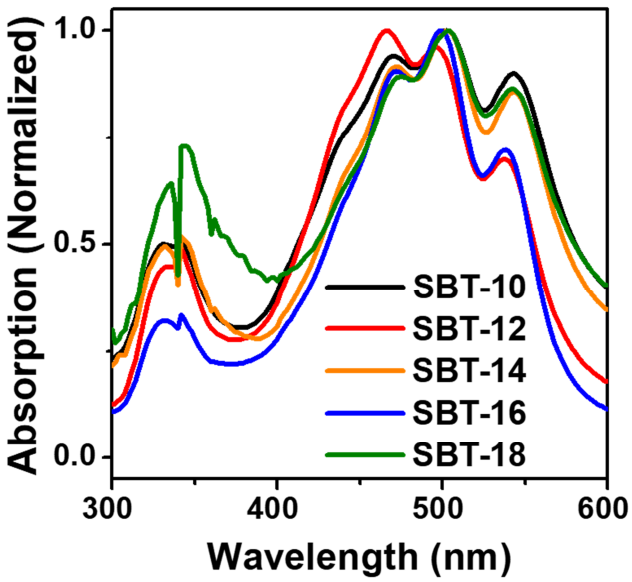

Fig. S3. UV-Vis spectra for spin-coated films of **SBT-10 – 18**.

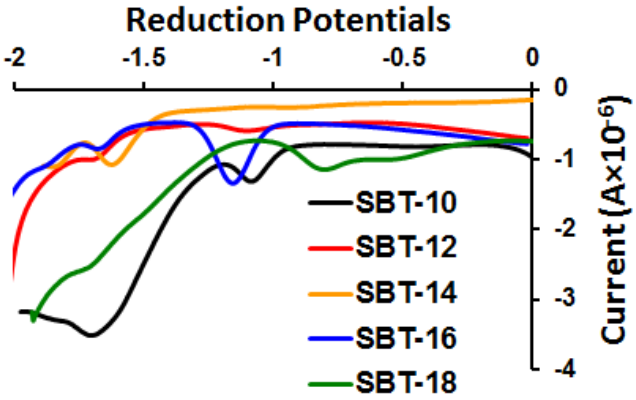

Fig. S4. Reduction potential curves of **SBT** compounds

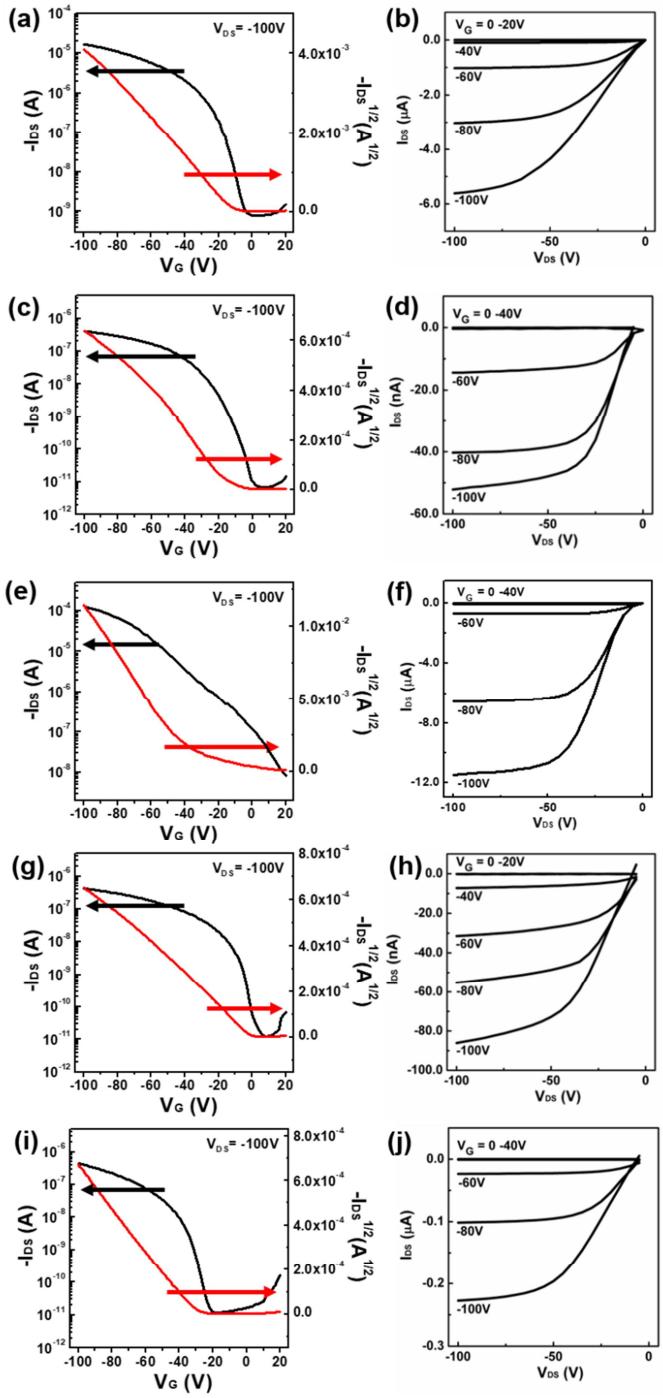

Fig. S5. Transfer and output characteristics of the TFT devices based on thin films of the compounds **SBT-10** (a, b), **SBT-12** (c, d), **SBT-14** (e, f), **SBT-16** (g, h), and **SBT-18** (i, j) employed in this study. (Measured in ambient and exhibited p-channel characteristics). Channel widths and lengths of 1000 μm and 50 μm were used, respectively for the devices.

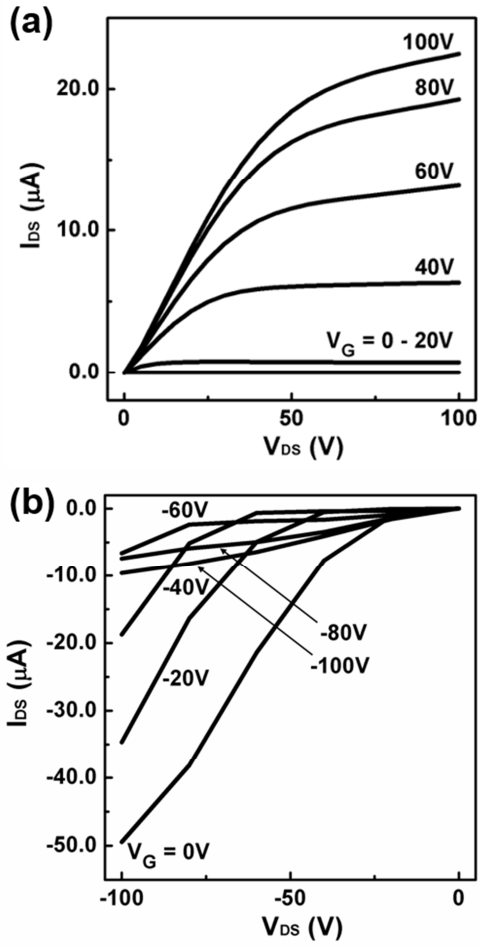

Fig. S6. (a) N type output curve (b) P type output curve of BHJ ambipolar transistors based on blends of **SBT-14** and **DTTRQ (C11)**.

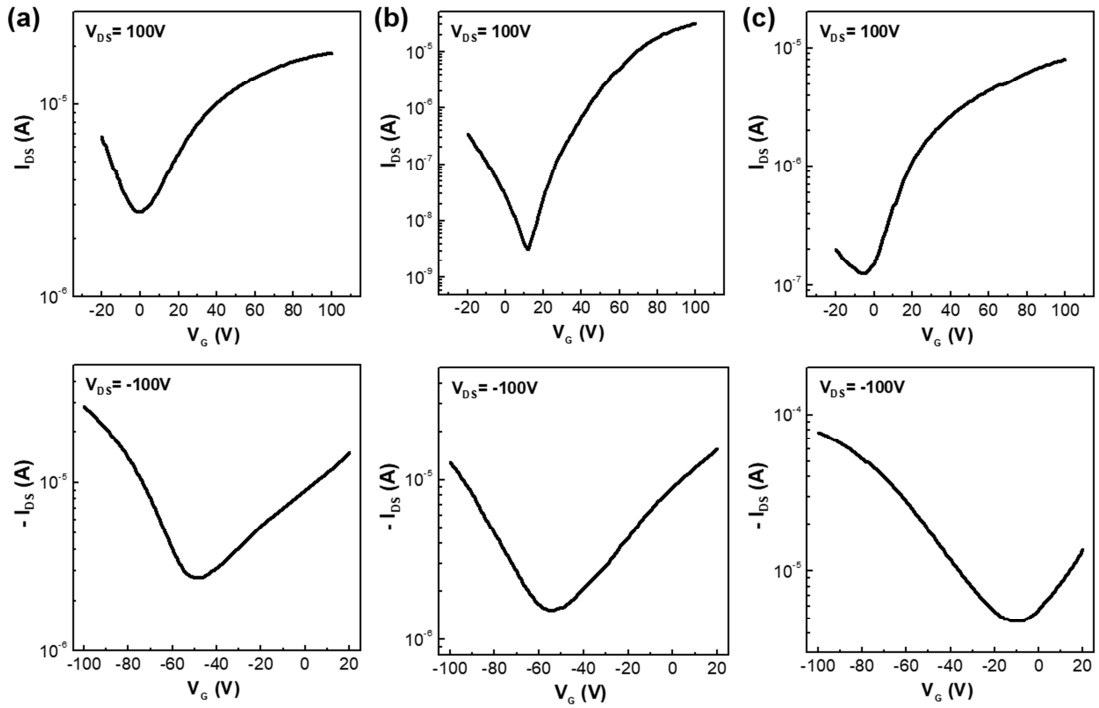

Fig. S7. (Top) N-channel and (Bottom) P–channel transfer characteristics of BHJ ambipolar transistors based on blends of **SBT-14** and (a) **DTTRQ (C3)**, (b) **DTTRQ (C6)**, and (c) **DTTRQ (C15)**. Channel widths and lengths of 1000 μm and 50 μm were used, respectively for (a), and channel widths and lengths of 1000 μm and 100 μm were used, respectively for (b) and (c).

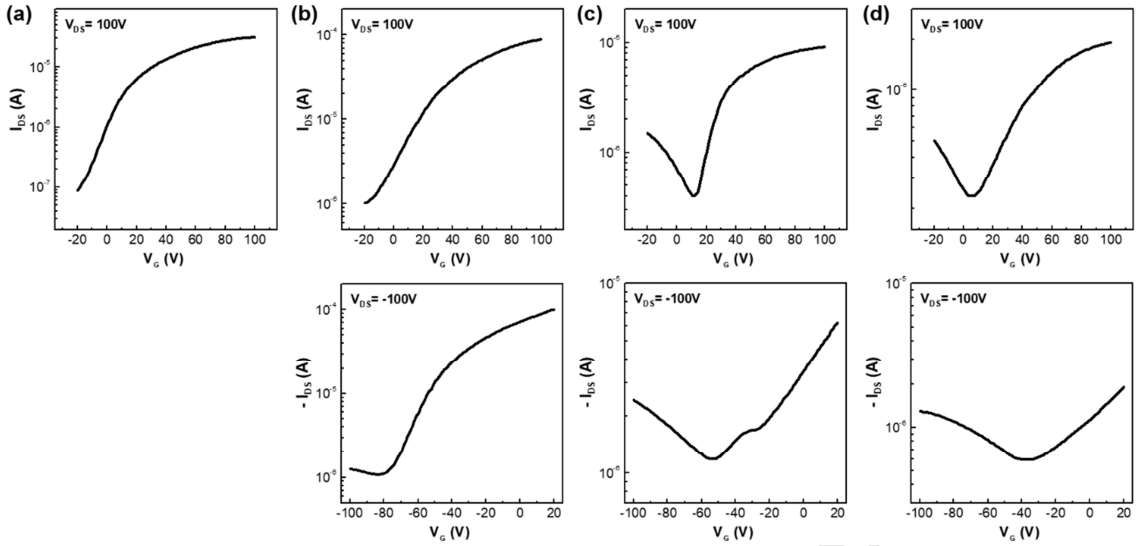

Fig. S8. (Top) N-channel and (Bottom) P–channel transfer characteristics of BHJ ambipolar transistors based on blends of **SBT-10** and (a) **DTTRQ (C3)**, (b) **DTTRQ (C6)**, (c) **DTTRQ (C11)**, and (d) **DTTRQ (C15)**. Channel widths and lengths of 1000 μm and 50 μm were used, respectively.

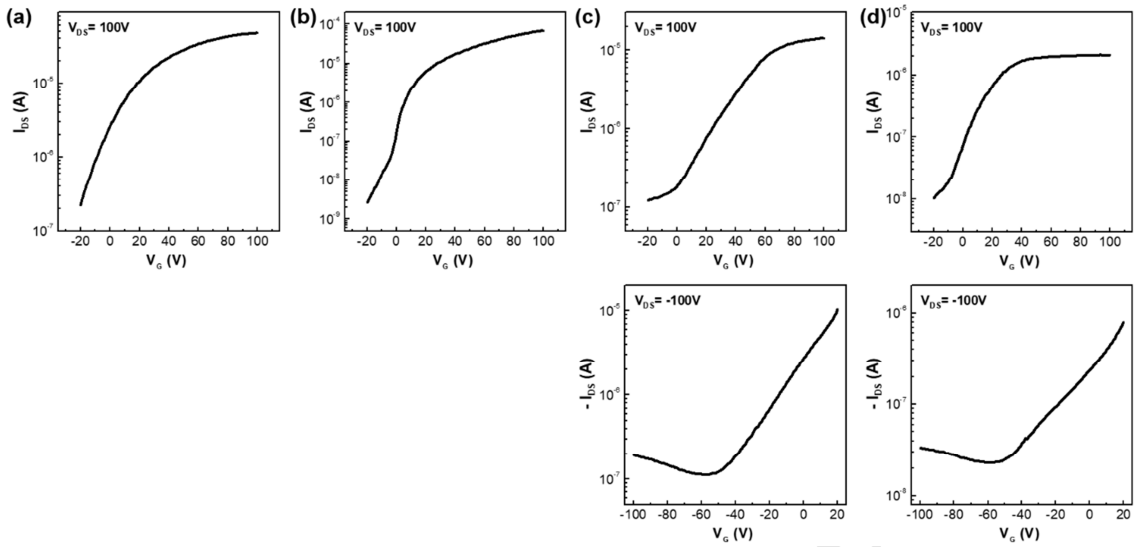

Fig. S9. (Top) N-channel and (Bottom) P–channel transfer characteristics of BHJ ambipolar transistors based on blends of **SBT-12** and (a) **DTTRQ (C3)**, (b) **DTTRQ (C6)**, (c) **DTTRQ (C11)**, and (d) **DTTRQ (C15)**. Channel widths and lengths of 1000 μm and 50 μm were used, respectively.

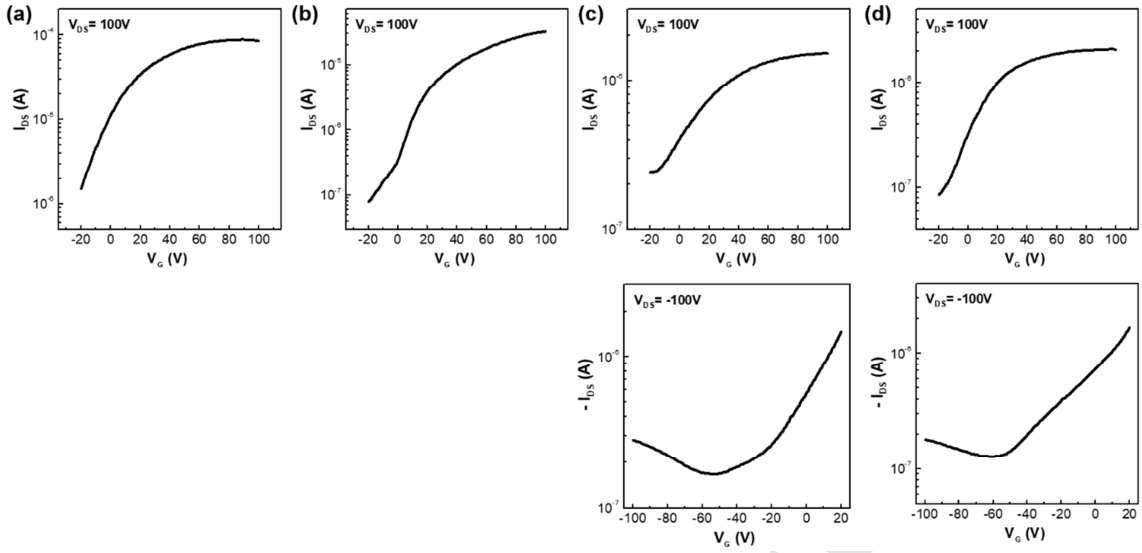

Fig. S10. (Top) N-channel and (Bottom) P–channel transfer characteristics of BHJ ambipolar transistors based on blends of **SBT-16** and (a) **DTTRQ (C3)**, (b) **DTTRQ (C6)**, (c) **DTTRQ (C11)**, and (d) **DTTRQ (C15)**. Channel widths and lengths of 1000 μm and 50 μm were used, respectively.

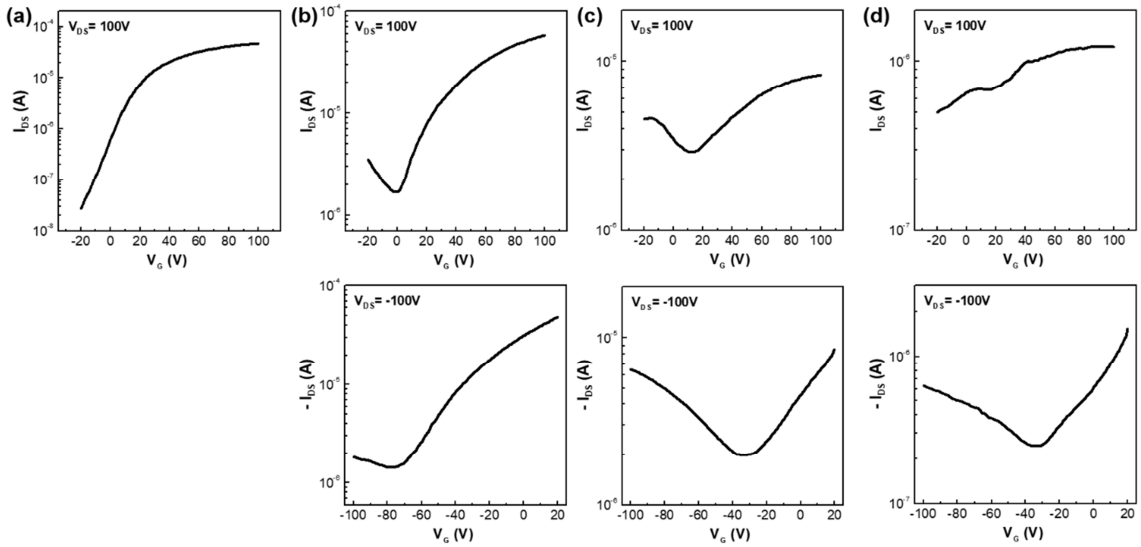

Fig. S11. (Top) N-channel and (Bottom) P–channel transfer characteristics of BHJ ambipolar transistors based on blends of **SBT-18** and (a) **DTTRQ (C3)**, (b) **DTTRQ (C6)**, (c) **DTTRQ (C11)**, and (d) **DTTRQ (C15)**. Channel widths and lengths of 1000 μm and 50 μm were used, respectively.

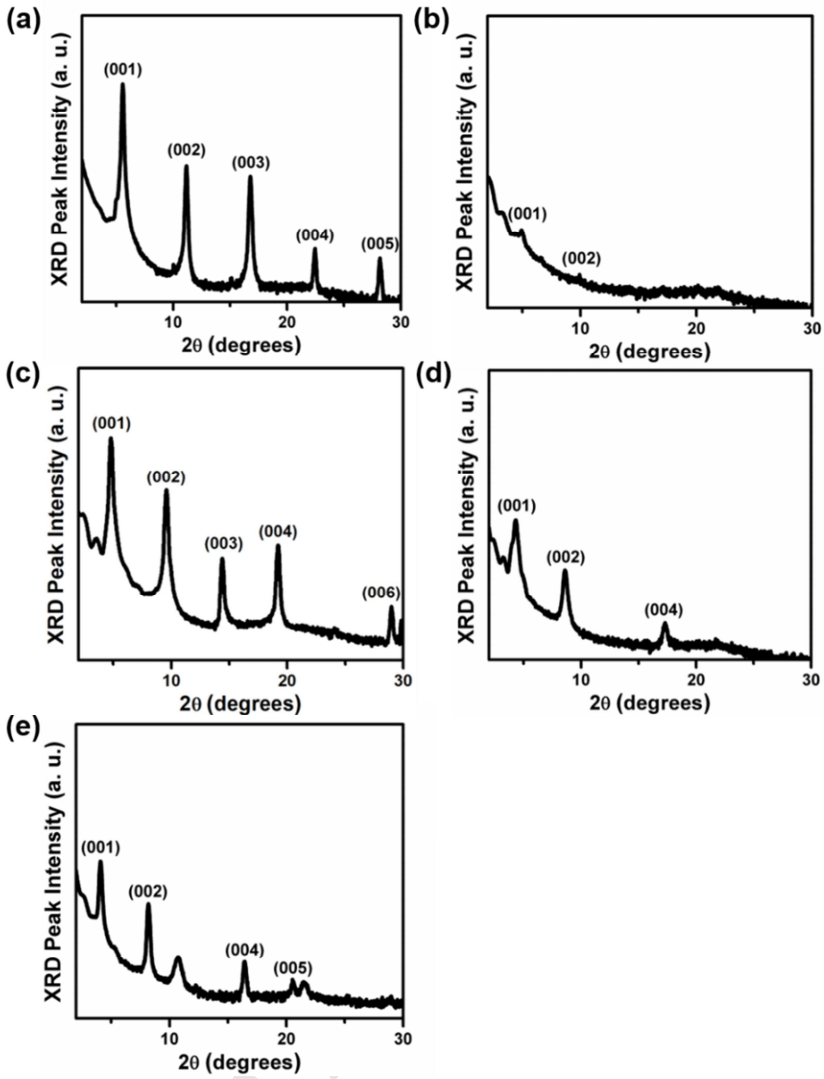

Fig. S12. θ-2θ X-ray diffraction (XRD) scans of solution-sheared thin films of **SBT-10** (a), **SBT-12** (b), **SBT-14** (c), **SBT-16** (d), and **SBT-18** (e).

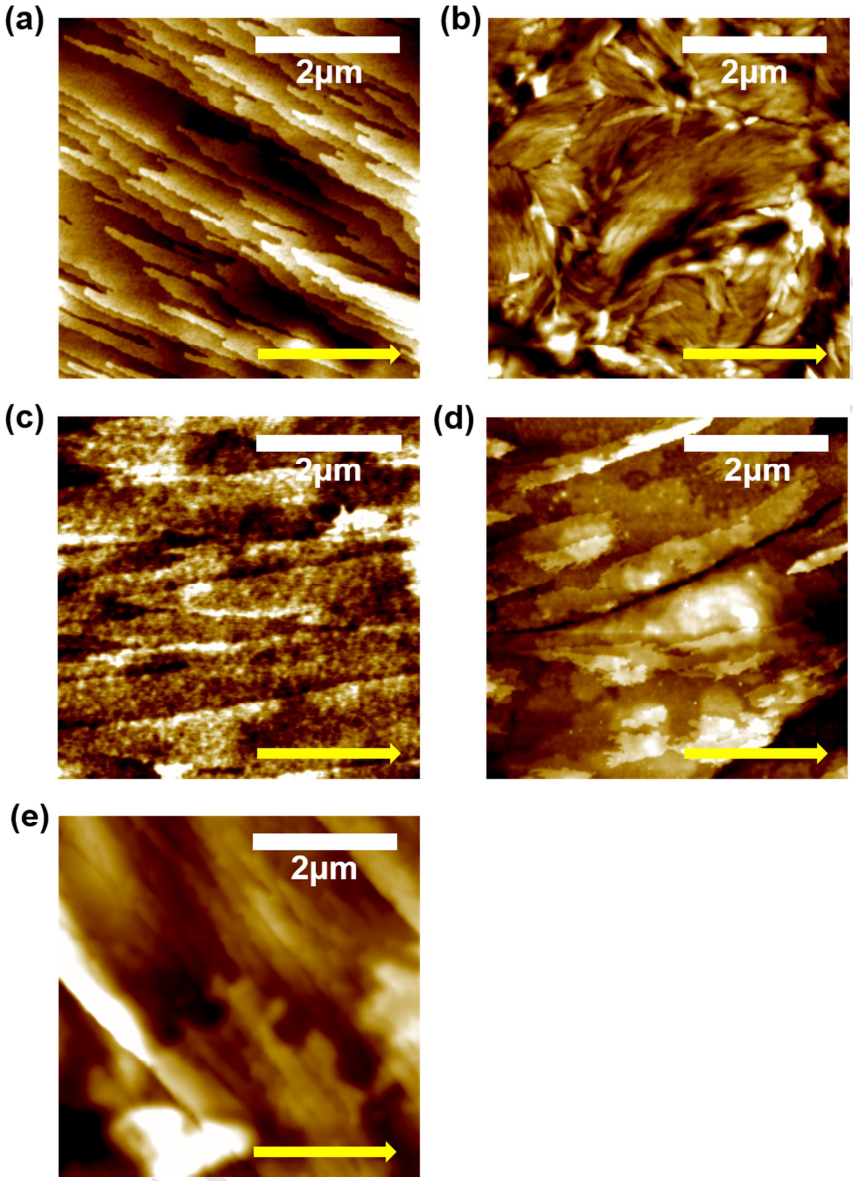

Fig. S13. Solution-sheared thin-film AFM topographic image of **SBT-10** (a), **SBT-12** (b), **SBT-14** (c), **SBT-16** (d), and **SBT-18** (e). Scale bar denotes 2 μm and the arrow shows the shearing direction.

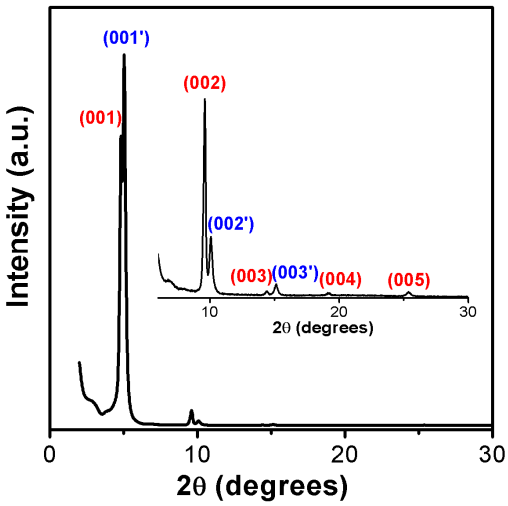

Fig. S14. *θ*-2*θ* X-ray diffraction (XRD) scans of BHJ thin film of **SBT-14:DTTRQ(C6) = 1:2**.

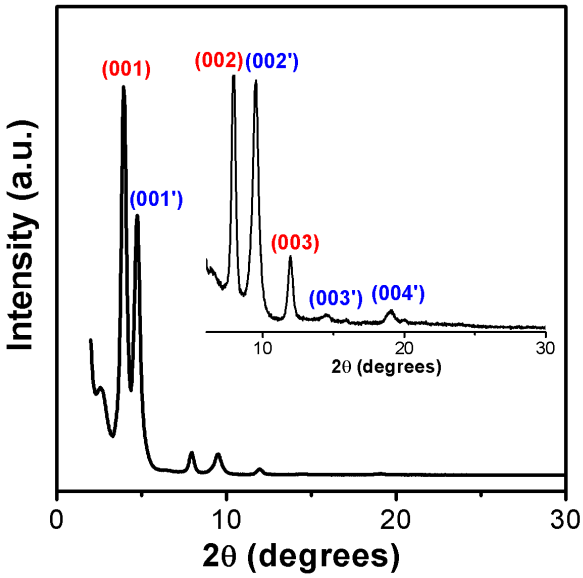

Fig. S15. *θ*-2*θ* X-ray diffraction (XRD) scans of BHJ thin film of **SBT-14:DTTRQ(C11) = 1:2**.

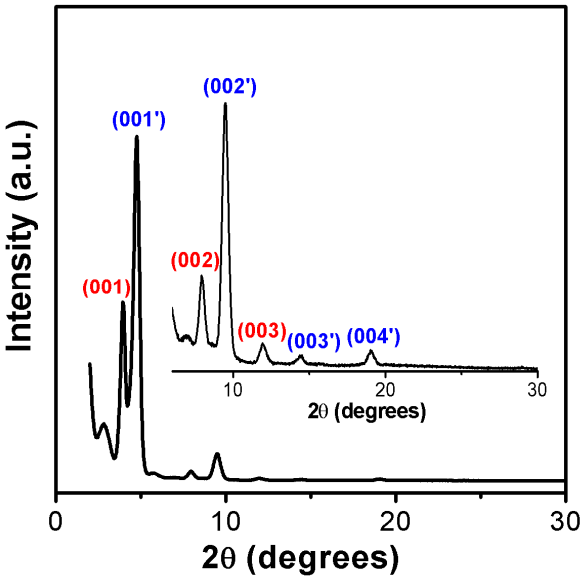

Fig. S16. θ-2θ X-ray diffraction (XRD) scans of BHJ thin film of **SBT-14:DTTRQ(C11) = 1:1**.

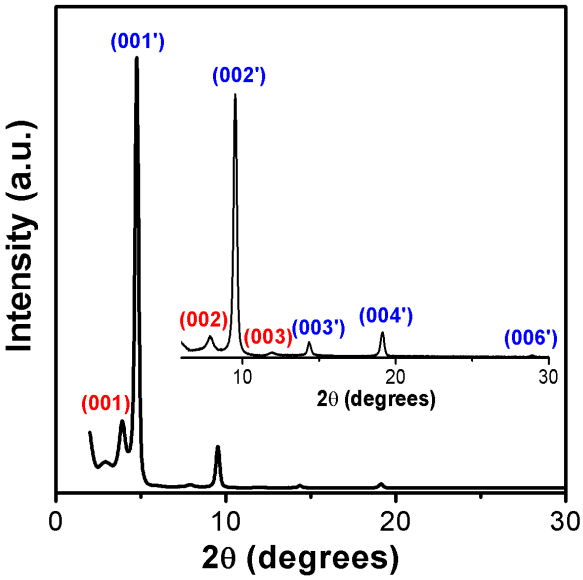

Fig. S17. *θ*-2*θ* X-ray diffraction (XRD) scans of BHJ thin film of **SBT-14:DTTRQ(C11) = 2:1**.

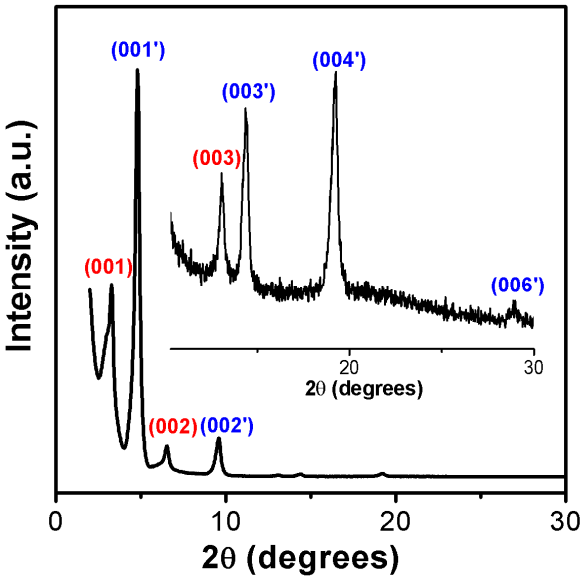

Fig. S18. θ-2θ X-ray diffraction (XRD) scans of BHJ thin film of **SBT-14:DTTRQ(C15) = 1:2**.

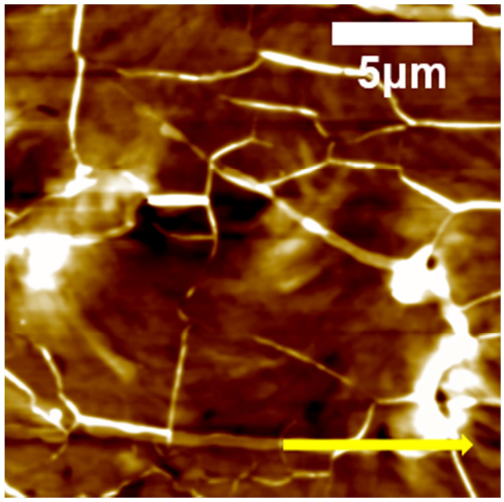

Fig. S19. BHJ thin-film AFM topographic image of **SBT-14**:**DTTRQ(C11)** = 1:1. Scale bar denotes 2 μm and the arrow shows the shearing direction.

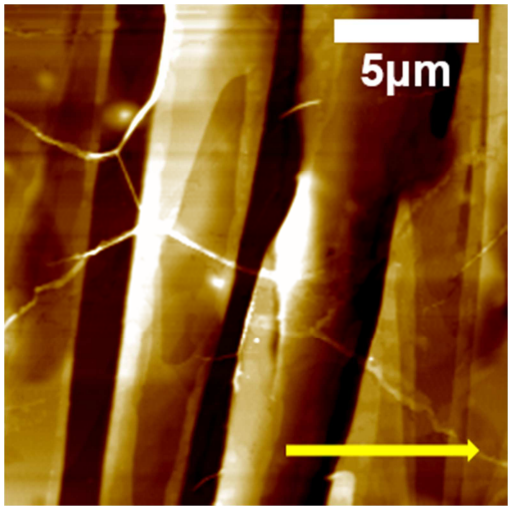

Fig. S20. BHJ thin-film AFM topographic image of **SBT-14**:**DTTRQ(C11)** = 2:1. Scale bar denotes 2 μm and the arrow shows the shearing direction.

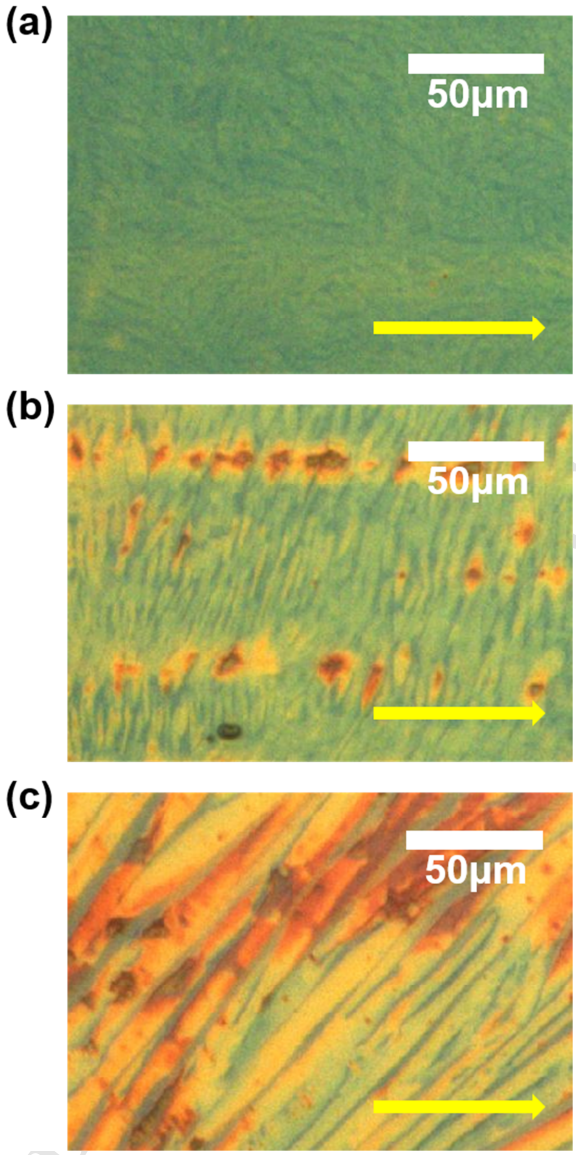

Fig. S21. Microscopy images for BHJ thin-film of **SBT-14**:**DTTRQ(C11)** = 1:2 (a), 1:1 (b), 2:1 (c). Scale bar denotes 50 μm and the arrow shows the shearing direction.

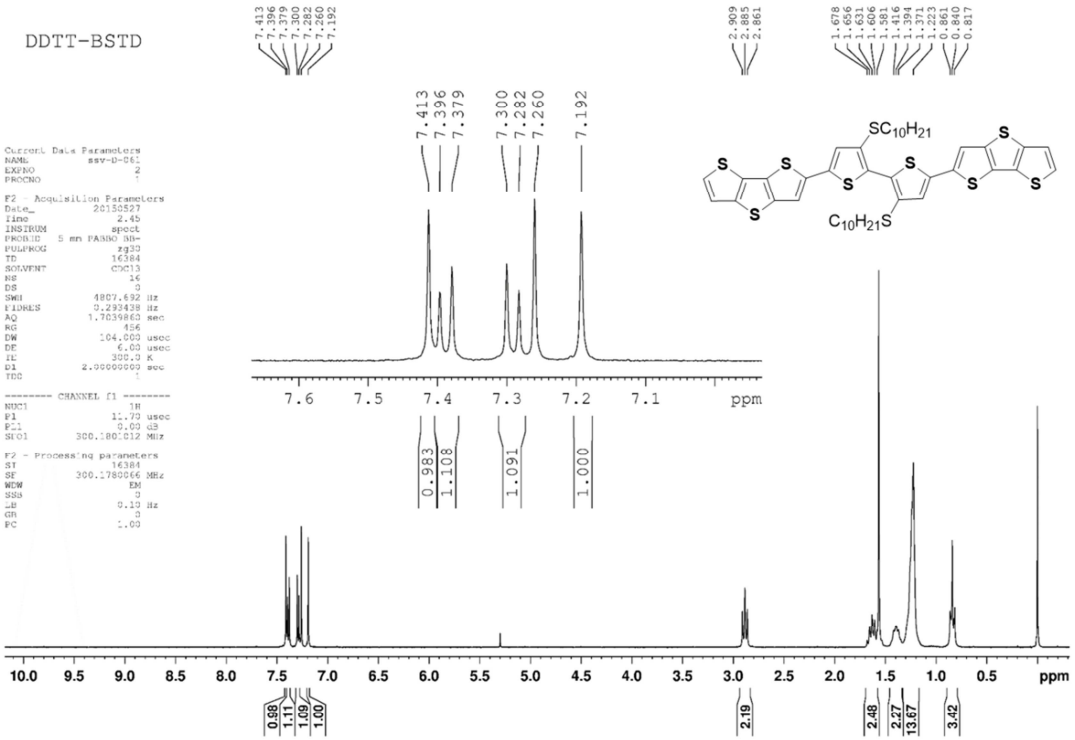

^{1}H NMR (300 MHz, CDCl3) spectrum of **SBT-10**.

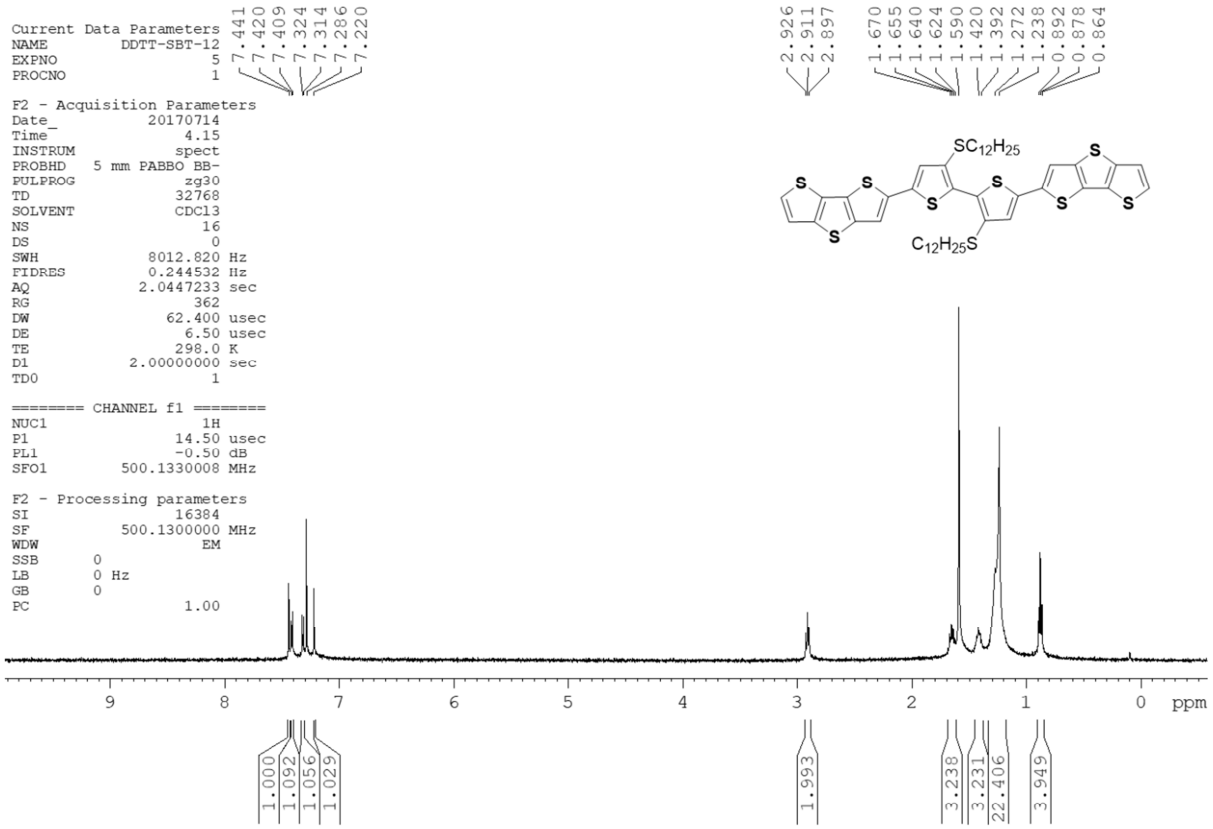

^{1}H NMR (500 MHz, CDCl3) spectrum of **SBT-12**.

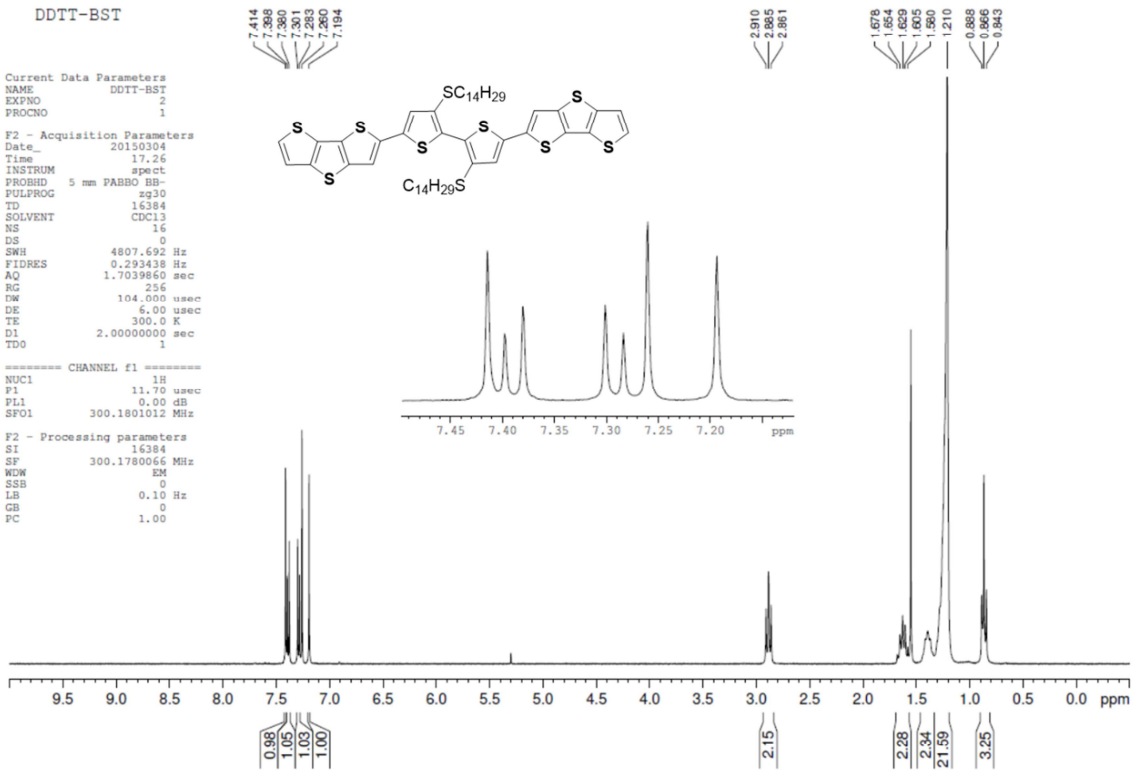

^{1}H NMR (300 MHz, CDCl3) spectrum of **SBT-14**.

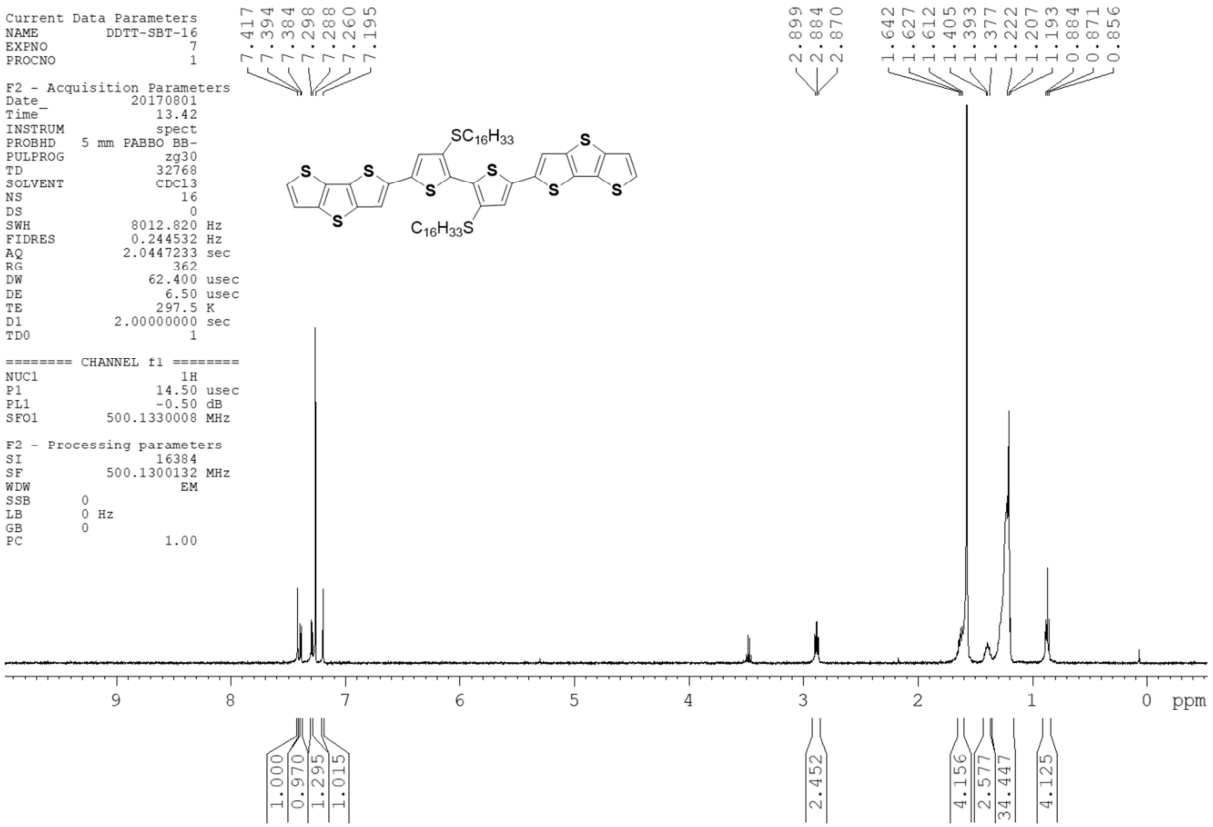

^{1}H NMR (500 MHz, CDCl3) spectrum of **SBT-16**.

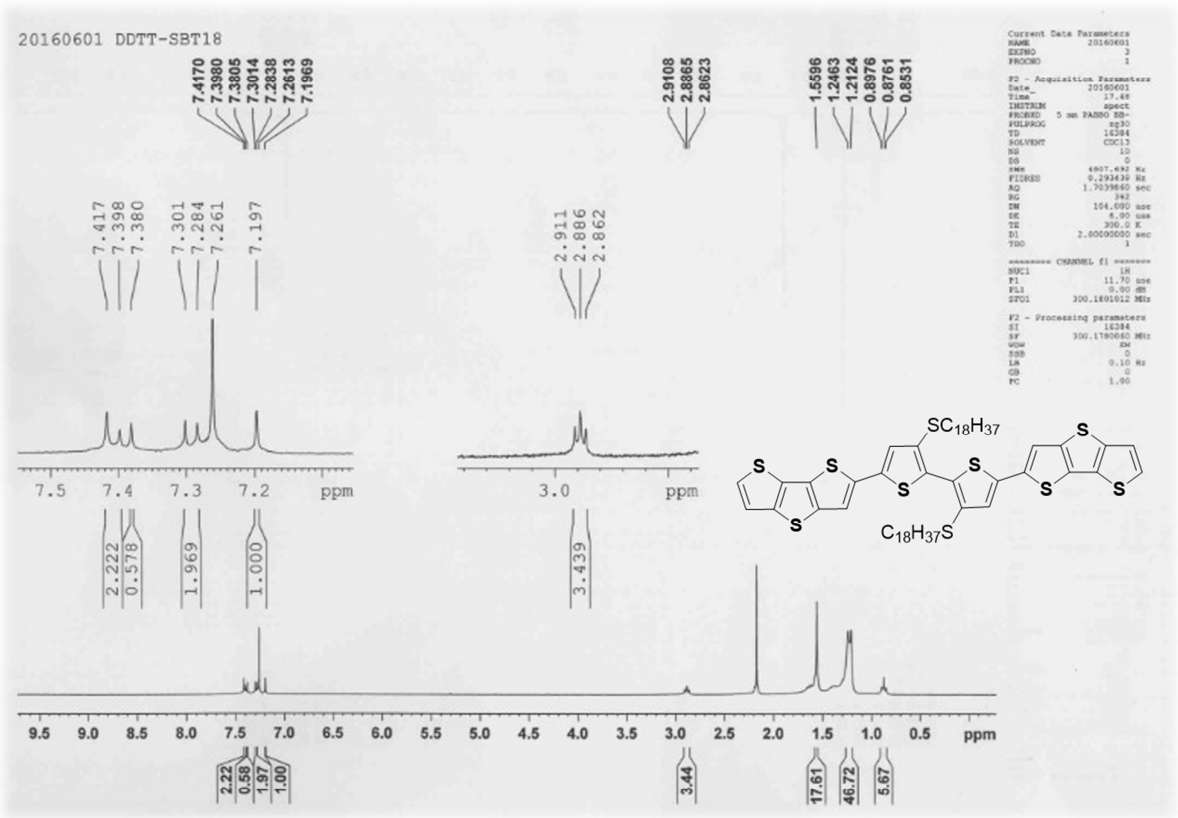

^{1}H NMR (300 MHz, CDCl3) spectrum of **SBT-18**.

Highlights:

• Solution-processable thioalkylated bithiophene derivatives are synthesized.

• Ambipolar transistors are fabricated based on bulk heterojunction small molecules.

• High electrical performance with carrier mobilities of 0.21 - 0.70 $cm^2 V^{-1} s^{-1}$ is achieved.

• Complementary-like inverters based on bulk-heterojunction transistors show high transfer gain of 81.